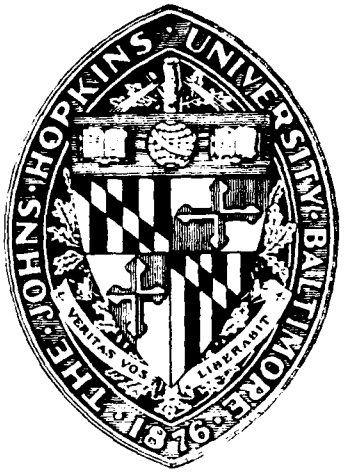

(2)

MATERIALS CHARACTERIZATION USING HOLOGRAPHIC MAPPING OF TRANSIENT LAMB WAVES

Michael J. Ehrlich and James W. Wagner, Ph.D. of the
Materials Science and Engineering Department
The Johns Hopkins University
Baltimore, Maryland 21218

TECHNICAL REPORT

ONR CONTRACT N00014-82-K-0741-PO4

FULL FIELD VISUALIZATION OF

SURFACE ACOUSTIC WAVES

September 1986

Prepared for

The Office of Naval Research

Physics Division, Code 1112

Arlington, Virginia 22217-5000

UNCLASSIFIED

SECURITY CLASSIFICATION OF THIS PAGE

(2)

REPORT DOCUMENTATION PAGE

Form Approved OMB No. 0704-0188

1a. REPORT SECURITY CLASSIFICATION: Unclassified	1b. RESTRICTIVE MARKINGS
2a. SECURITY CLASSIFICATION AUTHORITY	3. DISTRIBUTION / AVAILABILITY OF REPORT: Approved for public release; distribution unlimited
2b. DECLASSIFICATION / DOWNGRADING SCHEDULE	
4. PERFORMING ORGANIZATION REPORT NUMBER(S)	5. MONITORING ORGANIZATION REPORT NUMBER(S)
6a. NAME OF PERFORMING ORGANIZATION: The Johns Hopkins University; 6b. OFFICE SYMBOL (If applicable):	7a. NAME OF MONITORING ORGANIZATION: Office of Naval Research
6c. ADDRESS (City, State, and ZIP Code): Dept. of Materials Science & Engineering, 102 Maryland Hall, Baltimore, Maryland 21218	7b. ADDRESS (City, State, and ZIP Code): Physics Division, Code 1112, 800 North Quincy Street, Arlington, Virginia 22217-5000
8a. NAME OF FUNDING / SPONSORING ORGANIZATION; 8b. OFFICE SYMBOL (If applicable):	9. PROCUREMENT INSTRUMENT IDENTIFICATION NUMBER: N00014-82-K-0741-P04
8c. ADDRESS (City, State, and ZIP Code)	10. SOURCE OF FUNDING NUMBERS

PROGRAM ELEMENT NO.	PROJECT NO.	TASK NO.	WORK UNIT ACCESSION NO.
61153N.11		4126-813	

11. TITLE (Include Security Classification)
Materials Characterization Using Holographic Mapping of Transient Lamb Waves

12. PERSONAL AUTHOR(S)
Michael J. Ehrlich, M.S. and James W. Wagner, Ph.D.

13a. TYPE OF REPORT	13b. TIME COVERED	14. DATE OF REPORT (Year, Month, Day)	15. PAGE COUNT
Technical	FROM 8801 TO 8904	5/89	81

16. SUPPLEMENTARY NOTATION

17. COSATI CODES			18. SUBJECT TERMS (Continue on reverse if necessary and identify by block number)
FIELD	GROUP	SUB-GROUP	Flexural Waves; Holography; Holographic Interferometry; Acoustic Wave Visualization,
11	11/06	11/06/01	

19. ABSTRACT (Continue on reverse if necessary and identify by block number)

The testing of engineering materials is traditionally done using contact ultrasonic techniques or potentially destructive mechanical tests. For many materials, elastic properties are a function of both position and direction, owing to material anisotropy and inhomogeneities arising from process variation and defects. In order to determine these elastic properties as a function of position or direction using conventional techniques, it is necessary to scan the testing apparatus over the surface of the material.

In contrast, holographic methods offer a means of full field determination of the elastic properties. Toward this end, the spatial propagation of antisymmetric Lamb waves in nearly homogeneous isotropic plates has been investigated. Using high speed pulsed holographic techniques coupled with excitation of ultrasonic waves, surface displacements arising from Lamb wave propagation in thin plates result in interference patterns superimposed on the holographic reconstruction of the specimen image. The determination of

20. DISTRIBUTION / AVAILABILITY OF ABSTRACT	21. ABSTRACT SECURITY CLASSIFICATION
☒ UNCLASSIFIED/UNLIMITED ☐ SAME AS RPT ☐ DTIC USERS	UNCLASSIFIED

22a. NAME OF RESPONSIBLE INDIVIDUAL	22b. TELEPHONE (Include Area Code)	22c. OFFICE SYMBOL
L. E. Hargrove, ONR Physics Division	(202) 696-4221	ONR Code 1112

DD Form 1473, JUN 86 — Previous editions are obsolete.

SECURITY CLASSIFICATION OF THIS PAGE
UNCLASSIFIED

Block 19 continued

Lamb wave group velocities utilizing a technique which uses only features of the spatial waveform has been demonstrated to yield results in good agreement with elastic plate theory.

In addition, preliminary results show that the same holographic techniques may prove a useful tool in the characterization and evaluation of laminated composite plates.

MATERIALS CHARACTERIZATION USING HOLOGRAPHIC MAPPING OF TRANSIENT LAMB WAVES

Michael J. Ehrlich and James W. Wagner, Ph.D. of the
Materials Science and Engineering Department
The Johns Hopkins University
Baltimore, Maryland 21218

TECHNICAL REPORT

ONR CONTRACT N00014-82-K-0741-PO4

FULL FIELD VISUALIZATION OF

SURFACE ACOUSTIC WAVES

September 1986

Prepared for

The Office of Naval Research

Physics Division, Code 1112

Arlington, Virginia 22217-5000

Abstract

The testing of engineering materials is traditionally done using contact ultrasonic techniques or potentially destructive mechanical tests. For many materials, elastic properties are a function of both position and direction, owing to material anisotropy and inhomogeneities arising from process variation and defects. In order to determine these elastic properties as a function of position or direction using conventional techniques, it is necessary to scan the testing apparatus over the surface of the material.

In contrast, holographic methods offer a means of full field determination of the elastic properties. Toward this end, the spatial propagation of antisymmetric Lamb waves in nearly homogeneous isotropic plates has been investigated. Using high speed pulsed holographic techniques coupled with excitation of ultrasonic waves, surface displacements arising from Lamb wave propagation in thin plates result in interference patterns superimposed on the holographic reconstruction of the specimen image. The determination of Lamb wave group velocities utilizing a technique which uses only features of the spatial waveform has been demonstrated to yield results in good agreement with elastic plate theory.

In addition, preliminary results show that the same holographic technique may prove a useful tool in the characterization and evaluation of laminated composite plates.

Table of Contents

Table of Figures

Table of Tables

1 Introduction

Nondestructive testing of engineering materials has traditionally been done using contact ultrasonic techniques. These techniques typically utilize piezoelectric transducers which are mechanically coupled to the material surface. The transducers are used to generate acoustic waves within the material and to provide a means of detecting and recording the subsequent surface displacements resulting from the acoustic wave propagation. Such records of acoustic wave propagation within a material have been used to characterize material elastic properties[1.,2.].

Historically, ultrasonic methods used to determine elastic properties have been limited to recording surface displacements as a function of time for a single position on a material. However, for many materials, elastic properties are a function of both direction and position, owing to material anisotropy and inhomogeneities arising from process variation and defects. In order to determine the elastic properties as a function of direction using conventional ultrasonic techniques, it is necessary to scan the testing apparatus over the surface of the material. Unfortunately, this is both time consuming and potentially detrimental, in that the fluids necessary to couple the transducers to the material may contaminate the material or compromise the properties of the material surface.

In contrast to contact ultrasonic techniques, holography affords a means to provide a full field record of surface displacements as a function of position for a single instant in time. When coupled with ultrasonic excitation, holographic methods offer the ability to map surface displacements arising from propagating acoustic waves. As such, holographic/ultrasonic methods provide determination of material elastic properties as a function of position and direction. In addition, holographic detection of acoustic waves is a noncontact method, thus eliminating surface coupling effects and surface contamination.

Regardless of detection method, the determination of material elastic properties using acoustic wave propagation relies upon the ability to evaluate the velocities of characteristic acoustic modes. For a bulk unbounded medium, only two such modes are possible, namely the longitudinal and shear waves. Evaluation of elastic moduli using experimentally determined longitudinal and shear wave velocities is generally regarded as the most accurate method of material characterization. However, the geometry of many engineering materials and structures makes accurate determination of their elastic properties difficult when relying on bulk wave propagation techniques.

As the geometry of the medium becomes more complicated, i.e. free surfaces or layers are introduced, the number of possible acoustic modes increases, as does the complexity of particle motion associated with each mode. In particular, acoustic waves which propagate in other than bulk solids usually propagate as guided waves. Unlike bulk waves, the velocity of guided waves is generally dispersive in nature, i.e. a function of extrinsic factors such as specimen thickness or acoustic frequency. As such, the effect of these factors on guided wave propagation must be characterized before guided waves can be used for the determination of material elastic properties.

In order to gain a firm understanding of wave propagation in homogeneous isotropic solids, and how the measurement of such propagation may be applied to the characterization of materials, it is necessary to develop the wave equations which govern material particle motion. Toward this end, a derivation of the wave equation for bulk unbounded media is given and the behavior of bulk acoustic waves examined. Next, a single boundary condition is imposed which gives rise to the possibility of propagating surface acoustic waves, or Rayleigh waves, and this

type of wave behavior is described. Finally, a second boundary condition is imposed on the medium and the resulting modes of acoustic wave propagation, the Lamb modes, are discussed.

1.1 Wave Propagation in Unbounded Media

Consider a small volume element in the interior of a homogeneous isotropic medium. In general, stresses acting upon the element have components both normal and tangential to the element surfaces. Such stresses will be denoted σ_{ij}, where i denotes the direction in which the stress is acting, and j denotes the direction normal to the plane on which the stress is acting. It may be seen that for equilibrium, $\sigma_{xy} = \sigma_{yx}$, $\sigma_{zx} = \sigma_{xz}$, and $\sigma_{yz} = \sigma_{zy}$. Thus, only six independent components of stress exist. This is shown in Figure 1.1.1.

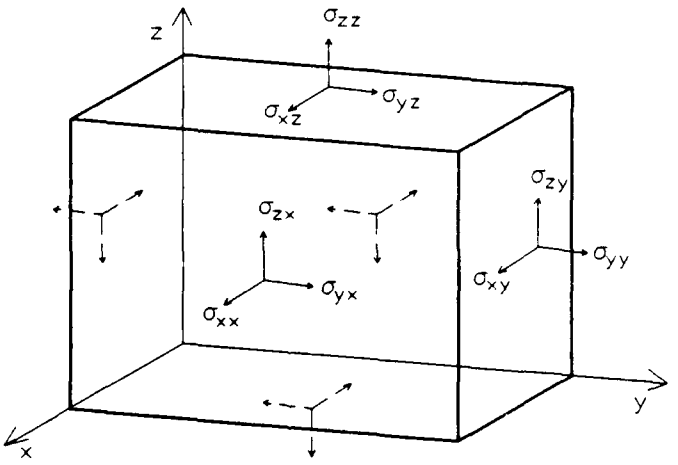

Figure 1.1.1. Volume element with associated stresses.

If a point P at location (x, y, z) within the body of the material is displaced, the displacement can be resolved into components (u, v, w) along the x, y, and z axes. Thus, the new location of point P is $(x+u, y+v, z+w)$. In order to describe the strain at P in the material, the displacement of points nearby P must be considered. If a

point Q at an initial location $(x+\delta x, y+\delta y, z+\delta z)$ nearby to P is displaced such that its displacement components are $(u+\delta u, v+\delta v, w+\delta w)$, and if $\delta x, \delta y, \delta z$ are small, the incremental displacements along x, y, and z are:

$$\delta u = \frac{\partial u}{\partial x}\delta x + \frac{\partial u}{\partial y}\delta y + \frac{\partial u}{\partial z}\delta z \tag{1.1.1a}$$

$$\delta v = \frac{\partial v}{\partial x}\delta x + \frac{\partial v}{\partial y}\delta y + \frac{\partial v}{\partial z}\delta z \tag{1.1.1b}$$

$$\delta w = \frac{\partial w}{\partial x}\delta x + \frac{\partial w}{\partial y}\delta y + \frac{\partial w}{\partial z}\delta z \tag{1.1.1c}$$

The nine quantities above can be regrouped as:

$$\epsilon_{xx} = \frac{\partial u}{\partial x} \qquad \epsilon_{yy} = \frac{\partial v}{\partial y} \qquad \epsilon_{zz} = \frac{\partial w}{\partial z} \tag{1.1.2a}$$

$$\epsilon_{yz} = \frac{\partial w}{\partial y} + \frac{\partial v}{\partial z} \qquad \epsilon_{zx} = \frac{\partial u}{\partial z} + \frac{\partial w}{\partial x} \qquad \epsilon_{xy} = \frac{\partial v}{\partial x} + \frac{\partial u}{\partial y} \tag{1.1.2b}$$

The quantities ϵ_{xx}, ϵ_{yy}, and ϵ_{zz} above represent the fractional extensions of the medium along the x, y, and z directions in the vicinity of P. These quantities are termed the longitudinal strain components. Similarly, the quantities ϵ_{yz}, ϵ_{zx}, and ϵ_{xy} represent the angular motions of the originally orthogonal volume element, and are termed the shear strain components[3]. In addition, three quantities which describe the rigid body rotation of the volume element can be defined:

$$2\bar{\Omega}_x = \frac{\partial w}{\partial y} - \frac{\partial v}{\partial z}, \qquad 2\bar{\Omega}_y = \frac{\partial u}{\partial z} - \frac{\partial w}{\partial x}, \qquad 2\bar{\Omega}_z = \frac{\partial v}{\partial x} - \frac{\partial u}{\partial y} \tag{1.1.2c}$$

where $\bar{\Omega}_i$ denotes rigid body rotation of the volume element about the i axis.

Considering only first order effects, each of the six components of stress (σ_{ij}) is a linear function of the six components of strain (ϵ_{ij}), where *i, j* denote the indices *x, y,* and *z*. This relationship is termed Hooke's law, and is detailed below:

$$\sigma_{xx} = c_{11}\epsilon_{xx} + c_{12}\epsilon_{yy} + c_{13}\epsilon_{zz} + c_{14}\epsilon_{yz} + c_{15}\epsilon_{zx} + c_{16}\epsilon_{xy} \quad (1.1.3a)$$

$$\sigma_{yy} = c_{21}\epsilon_{xx} + c_{22}\epsilon_{yy} + c_{23}\epsilon_{zz} + c_{24}\epsilon_{yz} + c_{25}\epsilon_{zx} + c_{26}\epsilon_{xy} \quad (1.1.3b)$$

$$\sigma_{zz} = c_{31}\epsilon_{xx} + c_{32}\epsilon_{yy} + c_{33}\epsilon_{zz} + c_{34}\epsilon_{yz} + c_{35}\epsilon_{zx} + c_{36}\epsilon_{xy} \quad (1.1.3c)$$

$$\sigma_{yz} = c_{41}\epsilon_{xx} + c_{42}\epsilon_{yy} + c_{43}\epsilon_{zz} + c_{44}\epsilon_{yz} + c_{45}\epsilon_{zx} + c_{46}\epsilon_{xy} \quad (1.1.3d)$$

$$\sigma_{zx} = c_{51}\epsilon_{xx} + c_{52}\epsilon_{yy} + c_{53}\epsilon_{zz} + c_{54}\epsilon_{yz} + c_{55}\epsilon_{zx} + c_{56}\epsilon_{xy} \quad (1.1.3e)$$

$$\sigma_{xy} = c_{61}\epsilon_{xx} + c_{62}\epsilon_{yy} + c_{63}\epsilon_{zz} + c_{64}\epsilon_{yz} + c_{65}\epsilon_{zx} + c_{66}\epsilon_{xy} \quad (1.1.3f)$$

The coefficients relating the stress to the strain are the elastic constants of the material. The elastic constants describe the behavior of the material when the material is placed under load. From above, there are 36 possible elastic constants, however it may be shown[4] that the elastic constant tensor must be symmetric, leaving 21 unique elastic constants. For materials that exhibit no particular spatial symmetry, all 21 constants are needed to completely describe the material's elastic behavior. For crystal systems that do exhibit varying degrees of symmetry, however, the number of elastic constants which must be specified to define the elastic properties is greatly reduced. In the case of cubic crystals, the elastic moduli tensor reduces to only three non-zero constants. In fact, for an isotropic material, only two elastic constants remain. These constants, λ and μ, are termed Lamé's constants, and are given by:

$$\lambda = c_{12} = c_{13} = c_{21} = c_{23} = c_{31} = c_{32} \quad (1.1.4)$$

$$\mu = c_{44} = c_{55} = c_{66}$$

$$\lambda + 2\mu = c_{11} = c_{22} = c_{33}$$

where the other 24 coefficients become zero.

For an isotropic material, λ and μ completely describe the elastic behavior. It is more common, however, to recognize four elastic constants for an isotropic solid. These are:

$E = \frac{\mu(3\lambda + 2\mu)}{\lambda + \mu}$ → Young's modulus is defined as the ratio between an applied stress and the corresponding strain in a direction parallel to the application of force. This is an extremely practical quantity, as it represents the stiffness of a material.

$\nu = \frac{\lambda}{2(\lambda + \mu)}$ → Poisson's ratio is defined as the ratio between the lateral contraction and longitudinal extension of the material subjected to a load.

$K = \lambda + \frac{2\mu}{3}$ → Bulk modulus is defined as the ratio between an applied hydrostatic pressure and the fractional volume change of the material due to the pressure. This may also be termed the modulus of incompressibility.

$\mu = \mu$ → Rigidity modulus is defined as the ratio between an applied shear stress and the resultant shear strain.

To obtain the equations of motion for such an isotropic solid, consider a variation in stress across a small volume element of the material. As shown in Figure 1.1.2, there are six separate components of force acting parallel to each axis. By Newton's second law of motion, the sum of the forces in any given direction must equal the mass of the volume element multiplied by the element's acceleration in that direction. Taking the sum of the forces in the x direction and setting it equal to mass times acceleration yields:

$$\left(\frac{\partial \sigma_{xx}}{\partial x}+\frac{\partial \sigma_{xy}}{\partial y}+\frac{\partial \sigma_{xz}}{\partial z}\right)\delta x\delta y\delta z=(\rho\delta x\delta y\delta z)\frac{\partial^2 u}{\partial t^2}$$

where ρ is the density of the volume element and u is the displacement in the x direction. This can be simplified to:

$$\rho\frac{\partial^2 u}{\partial t^2}=\frac{\partial \sigma_{xx}}{\partial x}+\frac{\partial \sigma_{xy}}{\partial y}+\frac{\partial \sigma_{xz}}{\partial z} \tag{1.1.5a}$$

In a similar fashion, the equations of motion for the v and w displacements are:

$$\rho\frac{\partial^2 v}{\partial t^2}=\frac{\partial \sigma_{yx}}{\partial x}+\frac{\partial \sigma_{yy}}{\partial y}+\frac{\partial \sigma_{yz}}{\partial z} \tag{1.1.5b}$$

$$\rho\frac{\partial^2 w}{\partial t^2}=\frac{\partial \sigma_{zx}}{\partial x}+\frac{\partial \sigma_{zy}}{\partial y}+\frac{\partial \sigma_{zz}}{\partial z} \tag{1.1.5c}$$

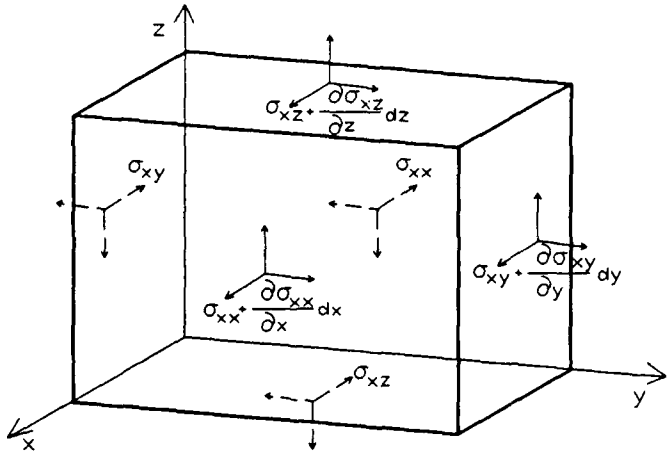

Figure 1.1.2 Stresses acting on a differential volume element in x direction.

The above equations of motion are true for any solid. To obtain a solution, the elastic relations between stress and strain must be applied. Defining the dilatation of a volume element as $\Delta = \epsilon_{xx} + \epsilon_{yy} + \epsilon_{zz}$ which is representative of the fractional volume change of the element, and substituting from 1.1.3 and 1.1.4 for σ_{xx}, σ_{xy}, and σ_{xz} in (1.1.5a) above yields:

$$\rho \frac{\partial^2 u}{\partial t^2} = \frac{\partial}{\partial x}(\lambda\Delta + 2\mu\epsilon_{xx}) + \frac{\partial}{\partial y}(\mu\epsilon_{xy}) + \frac{\partial}{\partial z}(\mu\epsilon_{xz})$$

Using the definitions of the strain components given in (1.1.2) yields:

$$\rho \frac{\partial^2 u}{\partial t^2} = (\lambda + \mu)\frac{\partial \Delta}{\partial x} + \mu\nabla^2 u \tag{1.1.6a}$$

where ∇^2 is the Laplacian operator. The results are similar for the v and w components of motion:

$$\rho \frac{\partial^2 v}{\partial t^2} = (\lambda + \mu)\frac{\partial \Delta}{\partial y} + \mu\nabla^2 v \tag{1.1.6b}$$

$$\rho \frac{\partial^2 w}{\partial t^2} = (\lambda + \mu)\frac{\partial \Delta}{\partial z} + \mu\nabla^2 w \tag{1.1.6c}$$

Thus, for an isotropic elastic solid, these are the equations of motion. For an unbounded medium, these equations correspond to two types of wave propagation. Differentiating both sides of (1.1.6a), (1.1.6b), and (1.1.6c) with respect to x, y, and z respectively, and adding yields:

$$\rho \frac{\partial^2 \Delta}{\partial t^2} = (\lambda + 2\mu)\nabla^2 \Delta \tag{1.1.7}$$

which is the wave equation for a dilatation propagated through the material with a velocity $V_L = \left(\frac{\lambda + 2\mu}{\rho}\right)^{\frac{1}{2}}$.

Eliminating the dilatation between (1.1.6b) and (1.1.6c) results in:

$$\rho \frac{\partial^2 \overline{\Omega}_x}{\partial t^2} = \mu \nabla^2 \overline{\Omega}_x \tag{1.1.8}$$

which is the wave equation for a solid body rotation about the x axis propagating with velocity $V_S = \left(\frac{\mu}{\rho}\right)^{\frac{1}{2}}$. Similar results are obtained for $\overline{\Omega}_y$, $\overline{\Omega}_z$.

Thus, waves involving no rotation are propagated through the interior of a material with velocity V_L. Such waves are termed longitudinal, dilatational or compressional waves. Waves involving no volume change, i.e. no dilatation, are propagated with a velocity V_S through the interior of a medium, and are called shear, transverse, or rotational waves. The particle motion in such waves is shown in Figure 1.1.3. It can be shown[5] that any plane wave propagated through the interior of an isotropic elastic medium must travel with one of the wave velocities detailed above. It should be noted that in general, these wave velocities are constants for a given material, independent of frequency or wavelength.

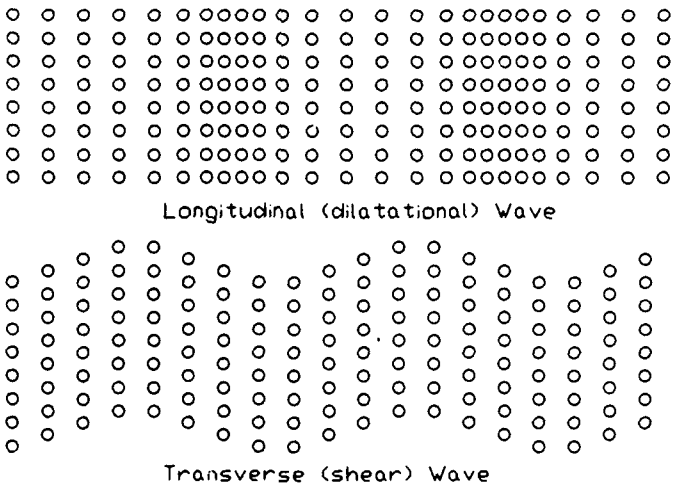

Figure 1.1.3 Particle motion in the interior of an isotropic solid due longitudinal and shear wave propagation

As noted earlier, elastic moduli are quite important from an engineering standpoint, as they describe the behavior of a given material under load. One method to determine the elastic moduli for a given material is to manufacture a tensile specimen of the material, load the sample to a known stress level, and measure the resulting strain in the direction of the applied load. Such a test is time consuming and potentially destructive, in that the sample may reach the realm of plastic strain during the test. Owing to this potential outcome, it is quite difficult to determine the elastic properties of a machined component using mechanical testing techniques.

Alternatively, the shear and longitudinal wave velocities can be measured for the material and from these measurements both λ and μ can be determined. Use of this technique to determine material elastic properties has a number of advantages over conventional mechanical tests. Most notably, measurement of wave velocities within a material is non-destructive. As such, completed components or structures can be tested for mechanical properties without fear of damage.

A number of techniques utilizing piezoelectric transducers are commonly employed to make such measurements. Although measurement of longitudinal and shear wave velocities by such methods provides an excellent means of testing and/or determining the elastic properties of materials, there are some situations where such measurements are impractical or impossible to make. For instance, the testing of structures with only a single accessible side requires the use of pulse-echo techniques[6]. Many ultrasonic transducers, however, have a finite "dead time" between generation and reception of acoustic waves. For thin structures, or very fast wave velocities, the pulse-echo travel time may exceed the reset time of the transducer,

resulting in poor or incorrect results. In addition, if a structure is very thick or the material very attenuative, it may prove difficult to measure bulk acoustic wave velocities owing to loss of signal.

1.2 Surface Acoustic Waves

Given an isotropic elastic solid, two types of bulk waves have been described, namely longitudinal and shear. If a boundary exists in the medium, it is possible to consider a plane wave propagating through the medium near the boundary and solve the equations of motion for such a condition. Waves of this type were first investigated by Lord Rayleigh in 1887, and subsequently termed Rayleigh waves. In an effort to describe such a wave, consider an elastic isotropic medium with a plane boundary located at $z=0$ *(x-y plane)* and assume a plane wave exists which travels in the x direction near this boundary and has components of motion only in the x-z plane, i.e. independent of y. The solution of the equations of motion (1.1.6) for such a wave must satisfy the condition that the boundary is free from stress. Since the displacements are independent of y, it is advantageous to define two potential functions ϕ and ψ such that:

$$u = \frac{\partial \phi}{\partial x} + \frac{\partial \psi}{\partial z} \qquad\qquad w = \frac{\partial \phi}{\partial z} - \frac{\partial \psi}{\partial x} \tag{1.2.1}$$

These potential functions are defined such that ϕ is associated with the dilatation produced by the wave whereas ψ is associated with the rotation. This can be seen by solving for the dilatation and rotation:

$$\Delta = \frac{\partial u}{\partial x} + \frac{\partial w}{\partial z} = \nabla^2 \phi$$

$$2\overline{\Omega}_y = \frac{\partial u}{\partial z} - \frac{\partial w}{\partial x} = \nabla^2 \psi$$

If, in fact, the particle motion for a surface wave is independent of y, then by substituting (1.2.1) into the equations of motion (1.1.6) using the potential functions described above, (1.1.6a) and (1.1.6c) become:

$$\rho\frac{\partial}{\partial x}\left(\frac{\partial^2\phi}{\partial t^2}\right)+\rho\frac{\partial}{\partial z}\left(\frac{\partial^2\psi}{\partial t^2}\right)=(\lambda+2\mu)\frac{\partial}{\partial x}(\nabla^2\phi)-\mu\frac{\partial}{\partial z}(\nabla^2\psi)$$

$$\rho\frac{\partial}{\partial z}\left(\frac{\partial^2\phi}{\partial t^2}\right)+\rho\frac{\partial}{\partial x}\left(\frac{\partial^2\psi}{\partial t^2}\right)=(\lambda+2\mu)\frac{\partial}{\partial z}(\nabla^2\phi)-\mu\frac{\partial}{\partial x}(\nabla^2\psi)$$

These equations will be satisfied if:

$$\frac{\partial^2\phi}{\partial t^2}=\left(\frac{\lambda+2\mu}{\rho}\right)\nabla^2\phi=V_L^2\nabla^2\phi \tag{1.2.2a}$$

$$\frac{\partial^2\psi}{\partial t^2}=\left(\frac{\mu}{\rho}\right)\nabla^2\psi=V_S^2\nabla^2\psi \tag{1.2.2b}$$

To search for a solution, consider a plane wave of frequency ω propagating in the x direction with a velocity V_R and wave number $k=2\pi/\Lambda$, where Λ is the wave-length, and assume a solution of (1.2.2) given by:

$$\phi=F(z)e^{i(\omega t-kx)} \tag{1.2.3a}$$

$$\psi=G(z)e^{i(\omega t-kx)} \tag{1.2.3b}$$

Here, *F(z)* and *G(z)* are amplitude functions dependent on z, the depth into the material surface, and detail how the wave amplitudes vary with z. If the above expressions are substituted into (1.2.2) above, the result is:

$$\frac{\partial^2}{\partial t^2}F(z)-(k^2-k_L^2)F(z)=0 \tag{1.2.4a}$$

$$\frac{\partial^2}{\partial t^2}G(z)-(k^2-k_S^2)G(z)=0 \tag{1.2.4b}$$

where

$$k_L = \frac{\omega}{V_L} \qquad k_S = \frac{\omega}{V_S} \tag{1.2.5a}$$

If the substitutions

$$q^2 = k^2 - k_L^2 \qquad s^2 = k^2 - k_S^2 \tag{1.2.5b}$$

are made above, the general solutions to (1.2.4) are

$$F(z) = Ae^{-qz} + A'e^{+qz} \tag{1.2.6a}$$

$$G(z) = Be^{-sz} + B'e^{+sz} \tag{1.2.6b}$$

The second term of each solution above is a function of e^z which corresponds to a wave whose amplitude increases with increasing z. However, a solution is sought which is confined to the boundary of the medium, one which decreases with increasing z, thus A' and B' are set to zero. Inserting (1.2.6) into (1.2.3) yields:

$$\phi = Ae^{-qz+i(\omega t-kx)} \tag{1.2.7a}$$

$$\psi = Be^{-sz+i(\omega t-kx)} \tag{1.2.7b}$$

Now that suitable solutions for ϕ and ψ have been found, it is necessary to satisfy the condition that at the boundary ($z=0$), all stresses must vanish. The boundary condition is therefor $\sigma_{zz} = \sigma_{zy} = \sigma_{zx} = 0$. From (1.1.3c),

$$\sigma_{zz} = \lambda\Delta + 2\mu\frac{\partial w}{\partial z}$$

and using (1.2.1), this becomes:

$$\sigma_{zz} = (\lambda + 2\mu)\frac{\partial^2\phi}{\partial z^2} + \lambda\frac{\partial^2\phi}{\partial x^2} - 2\mu\frac{\partial^2\psi}{\partial z\partial x}$$

Substituting in the expression for ϕ and ψ from (1.2.7), and solving at $z=0$ gives:

$$A\{(\lambda + 2\mu)q^2 - \lambda k^2\} - 2B\mu isk = 0 \tag{1.2.8}$$

Also from (1.1.3e), using (1.2.1):

$$\sigma_{zx} = \mu\left(\frac{\partial u}{\partial z} + \frac{\partial w}{\partial x}\right) = \mu\left(2\frac{\partial^2 \phi}{\partial z \partial x} - \frac{\partial^2 \psi}{\partial x^2} + \frac{\partial^2 \psi}{\partial z^2}\right)$$

Again, substituting in for ϕ and ψ at $z=0$ yields:

$$2iqkA + (s^2 + k^2)B = 0 \tag{1.2.9}$$

Equations (1.2.8) and (1.2.9) can be simplified by eliminating A and B and substituting in for q and s to give:

$$16\mu^2(k^2 - k_L^2)(k^2 - k_S^2)k^4 = \{-(\lambda + 2\mu)k_S^2 + 2\mu k^2\}^2(2k^2 - k_S^2)^2 \tag{1.2.10}$$

Finally, (1.2.10) can be expressed in terms of V_L, V_S and V_R by substituting in for k, k_L and k_S. Equation (1.2.10) then becomes:

$$\left(\frac{V^2}{V_S^2}\right)^3 - 8\left(\frac{V^2}{V_S^2}\right)^2 + 24\left(\frac{V^2}{V_S^2}\right) - 16\left(\frac{V^2}{V_L^2}\right) + 16\left(\frac{V_S^2}{V_L^2}\right) - 16 = 0 \tag{1.2.11}$$

This is the Rayleigh equation, and gives the velocity of propagation of a surface wave (Rayleigh wave) as a function of the bulk longitudinal and shear wave velocities. It is clear that the velocity of propagation of the Rayleigh wave V_R is independent of frequency, and is indeed only a function of the elastic properties of the material. As such, Rayleigh waves are useful in determining surface material elastic properties or characterizing surface layers[7]. For real materials, V_R must fall between 87% and 96% of the bulk shear wave velocity[8]. In addition, the amplitude of the Rayleigh wave in the z direction (into the material) goes as[9]:

$$e^{-\sqrt{k^2 - k_L^2}\cdot z} - \frac{2k^2}{2k^2 - k_S^2}e^{-\sqrt{k^2 - k_S^2}\cdot z}$$

This is a function which increase in the material and reaches a maximum at approximately 10% of the Rayleigh wavelength, then decreases monotonically with increasing depth. At a depth approximately equal to one wavelength, the Rayleigh wave amplitude is only 20% of its surface value. In effect, the wave is confined to the material surface.

By introducing a plane boundary on an isotropic elastic solid, and solving the equations of motion for the condition that all stresses at the boundary must go to zero, the existence of a Rayleigh wave has been shown. The Rayleigh wave is constrained to the surface of the material, and travels with a velocity between $0.87V_S$ and $0.96V_S$, dependent upon the material elastic constants.

1.3 Lamb Waves

In 1916 a theory on the propagation of acoustic waves in plates was presented by Horace Lamb to the Royal Society of London[10]. The theory was developed assuming a perfectly elastic, homogeneous and isotropic medium, in which particle displacements occur only in the plane containing the wave propagation vector and the normal to the plate surface. Following the approach by Lamb, using (1.1.2) and (1.1.3), and referring to Figure 1.3.1, the relevant stress strain relations in the plate are given by:

$$\sigma_{zz} = \lambda\left(\frac{\partial u}{\partial x} + \frac{\partial w}{\partial z}\right) + 2\mu\frac{\partial u}{\partial z} \tag{1.3.1a}$$

$$\sigma_{xz} = \mu\left(\frac{\partial w}{\partial x} + \frac{\partial u}{\partial z}\right) \tag{1.3.1b}$$

As for Rayleigh waves, the solution of the above equations takes the form identical to (1.2.1):

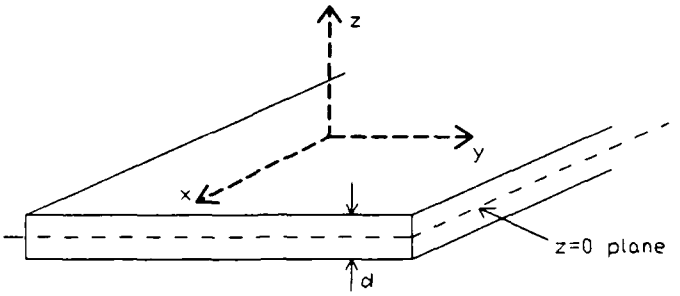

Figure 1.3.1 Coordinate system used for plate wave development.

$$u = \frac{\partial \phi}{\partial x} + \frac{\partial \psi}{\partial z} \qquad w = \frac{\partial \phi}{\partial z} - \frac{\partial \psi}{\partial x} \tag{1.3.2}$$

where ϕ, ψ are scalar potential functions. As per the Rayleigh wave derivation, these potential functions must satisfy

$$\frac{\partial^2 \phi}{\partial t^2} = \left(\frac{\lambda + 2\mu}{\rho}\right)\nabla^2 \phi = V_L^2 \nabla^2 \phi \tag{1.3.3a}$$

$$\frac{\partial^2 \psi}{\partial t^2} = \left(\frac{\mu}{\rho}\right)\nabla^2 \psi = V_S^2 \nabla^2 \psi \tag{1.3.3b}$$

It is apparent from Section 1.1 that the above relationships are the wave equations associated with dilatational and rotational waves, respectively. In solving for ϕ and ψ a plane wave solution is assumed, such that there is no y dependence of the particle motion. In addition, it is assumed that potential functions are periodic with time and in the x direction. Such a periodic dependence introduces the factors $e^{i\omega t}$ and e^{ikx} in the solutions for ϕ and ψ. Recalling k_L and k_S as defined in (1.2.5a), and using the time periodicity of the functions, the wave equations (Eq. (1.3.3) become:

$$(\nabla^2 + k_L^2)\phi = 0 \tag{1.3.4a}$$

$$(\nabla^2 + k_S^2)\psi = 0 \tag{1.3.4b}$$

Next, using the periodicity of the potential functions with x, the wave equations (Eq. 1.3.4) become:

$$\frac{\partial^2 \phi}{\partial z^2} = q^2 \phi \tag{1.3.5a}$$

$$\frac{\partial^2 \psi}{\partial z^2} = s^2 \psi \tag{1.3.5b}$$

where q and s are as defined in (1.2.5b). Solutions of this equation set are:

$$\phi = (A \cosh qz) e^{ikx} \tag{1.3.6a}$$

$$\psi = (B \sinh sz) e^{ikx} \tag{1.3.6b}$$

and

$$\phi = (C \sinh qz) e^{ikx} \tag{1.3.7a}$$

$$\psi = (D \cosh sz) e^{ikx} \tag{1.3.7b}$$

Examination of the solution set above reveals that the potential function solutions which follow (1.3.6) are symmetric with respect to the median plane *(z=0)* of the plate. Likewise, the potential functions which follow (1.3.7) are anti-symmetric with respect to the median plane.

Using (1.3.2) and (1.3.5), and substituting these into the original stress-strain relationships (1.3.1) results in:

$$\frac{\sigma_{zz}}{\mu} = (k^2 + s^2)\phi - 2ik\frac{\partial \psi}{\partial z} \tag{1.3.8a}$$

$$\frac{\sigma_{xz}}{\mu} = 2ik\frac{\partial \phi}{\partial z} + (k^2 + s^2)\psi \tag{1.3.8b}$$

The derivation from this point for both symmetric and anti-symmetric modes is similar, however only the anti-symmetric solutions (1.3.7) will be explicitly derived.

It is at this point in the development that the derivation diverges from that of a bulk material or Rayleigh waves, in that a second boundary condition is applied which takes into account the geometry of the plate. Solving for the stresses at the plate boundaries, $z = \pm\frac{d}{2}$, by substituting (1.3.7) into (1.3.8) results in:

$$\frac{\sigma_{zz}}{\mu} = \pm\left[A(k^2+s^2)\sinh q\frac{d}{2} - 2iBks\sinh s\frac{d}{2}\right]e^{ikx} \tag{1.3.9a}$$

$$\frac{\sigma_{xz}}{\mu} = \left[2iAkq\cosh q\frac{d}{2} + B(k^2+s^2)\cosh s\frac{d}{2}\right]e^{ikx} \tag{1.3.9b}$$

Since the plate surfaces are free, all components of stress must go to zero at the plate boundaries. Equating the stress states above (1.3.9) to zero, and eliminating the constants A,B yields the characteristic equation for anti-symmetric Lamb modes:

$$\frac{\tanh\left(s\frac{d}{2}\right)}{\tanh\left(q\frac{d}{2}\right)} = \frac{(k^2+s^2)^2}{4k^2qs} \tag{1.3.10}$$

Substituting the values for q, s and k into (1.3.10), yields the characteristic equation for anti-symmetric Lamb wave velocity in terms of V_L, V_S as

$$\frac{\tanh\left\{\pi fd\sqrt{\frac{V_S^2-V^2}{V_S^2V^2}}\right\}}{\tanh\left\{\pi fd\sqrt{\frac{V_L^2-V^2}{V_L^2V^2}}\right\}} = \frac{\left(2-\frac{V^2}{V_S^2}\right)^2}{4\sqrt{\left(1-\frac{V^2}{V_L^2}\right)\left(1-\frac{V^2}{V_S^2}\right)}} \tag{1.3.11}$$

where $f = \frac{\omega}{2\pi}$ is the Lamb wave frequency, d is the plate thickness, and V is the Lamb wave velocity.

Upon examination of the Lamb equation (1.3.11), it is apparent if $V > V_S$, the hyperbolic tangent argument in the numerator becomes imaginary. Using the fact that $\tanh(ix) = \tan(x)/i$, this results in an infinite number of roots for the product fd, owing to the periodicity of the *tan()* function. Physically, this means that at a given

fixed frequency, a number of waves may propagate in the plate, each with a different phase velocity. However, for $V < V_S$ and $fd \to 0$, there exists only a single root to the characteristic Lamb wave equation. This root is termed the lowest order anti-symmetric mode (A_0). It is also evident from the Lamb equation (1.3.11) that Lamb wave phase velocity is a function of the frequency-plate thickness product. It is this dependence that makes Lamb waves unique. Neither shear, longitudinal, nor surface waves exhibit any type of frequency dispersion. In the limit where $fd \to \infty$, the *tanh()* functions go to a value of 1, and the wave equation becomes[11]:

$$\left(\frac{V^2}{V_S^2}\right)^3 - 8\left(\frac{V^2}{V_S^2}\right)^2 + 24\left(\frac{V^2}{V_S^2}\right) - 16\left(\frac{V^2}{V_L^2}\right) + 16\left(\frac{V_S^2}{V_L^2}\right) - 16 = 0 \qquad (1.3.12)$$

This is the Rayleigh wave equation, as previously derived, which yields solutions for waves which propagate along the surface of a medium, and are exponentially attenuated in a direction normal to the surface. Thus, for large *fd* products, the lowest order anti-symmetric lamb mode, as well as the lowest order symmetric mode, propagate with a phase velocity equal to the Rayleigh velocity, and are indistinguishable from Rayleigh waves[12].

Figure 1.3.2 plots the anti-symmetric Lamb equation (phase velocity normalized by shear velocity as a function of the frequency-plate thickness product) for brass. In addition, the group velocity of the Lamb wave $\left(V_G = \left[V - \lambda \frac{\partial V}{\partial \lambda}\right]\right)$ is also plotted. From this figure, it is clear that in the limit $fd \to \infty$, both the phase and group velocity of the Lamb wave approach that of the Rayleigh surface wave.

To further describe Lamb waves, it is necessary to examine the plate motion during the propagation of such a wave. As stated earlier, the solutions of (1.3.5) take both a symmetric (1.3.6) and anti-symmetric (1.3.7) form. It has been shown[13] that the overall plate motion for these solutions is as illustrated in Figure 1.3.3.

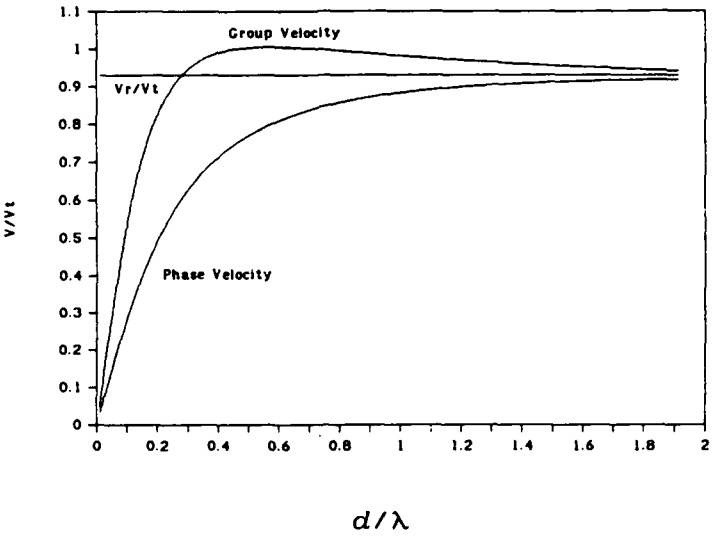

Figure 1.3.2 Anti-symmetric Lamb wave phase and group velocity dispersion relationships.

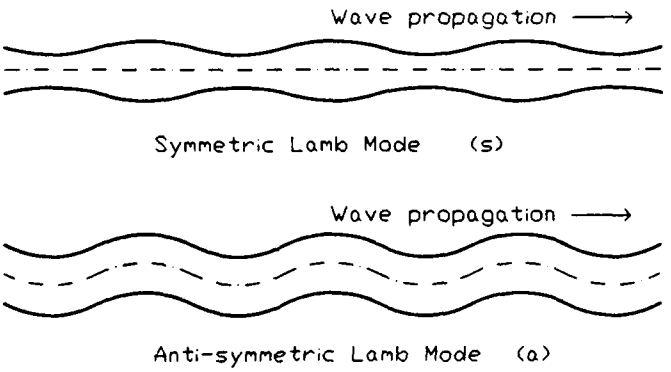

Figure 1.3.3 Plate motion for symmetric (s) and anti-symmetric (a) modes of Lamb wave propagation.

In order to describe the motion of particles within the plate during Lamb wave propagation, the solutions to the wave equation (1.3.6, 1.3.7) can be substituted back into the displacement equations (1.3.2). For the symmetric solution, this yields:

$$u = (ikA\cosh qz + sB\cosh \beta z)e^{ikx} \qquad (1.3.13a)$$

$$w = (qA\sinh qz - ikB\sinh sz)e^{ikx} \tag{1.3.13b}$$

And for the anti-symmetric case:

$$u = (ikC\sinh qz + sD\sinh sz)e^{ikx} \tag{1.3.14a}$$

$$w = (qC\cosh qz - ikD\cosh sz)e^{ikx} \tag{1.3.14b}$$

If these equations are evaluated for particle motion in the median plane of the plate *(z=0)*, we find that there is no *z* component of motion for symmetric modes, and the median plane particle motion obeys:

$$u = (ikA + sB)e^{ikx}$$

This represents a plane wave propagating along the *x* axis - a pure longitudinal wave. For the anti-symmetric case, there is no *u* component of motion for median plane particles, and we have:

$$w = (qC - ikD)e^{ikx}$$

This equation represents a wave propagating along the *x* axis, with particle displacement only along the *z* axis - a purely transverse wave.

As shown, particles lying in the median plane of the plate exhibit pure mode longitudinal wave behavior for symmetric Lamb modes, and pure mode shear wave behavior for anti-symmetric Lamb modes. In general, however, particles which reside away from the median plane experience motion due to the presence of both shear and longitudinal waves, and thus have a more complicated behavior. For symmetric modes, particle motion is predominantly along the *x* axis, with the small transverse displacements reaching a maximum at the plate surface and gradually going to zero in the median plane. For anti-symmetric modes, particle motion is predominantly in the transverse *(z)* direction, with the small longitudinal displacements reaching a maximum at the plate surface and gradually going to zero in the

median plane[14]. At the plate boundaries, particles follow an elliptical orbit, with the major axis of the ellipse dependent on whether a symmetric or antisymmetric mode is propagating[15]. This is shown in Figure 1.3.4.

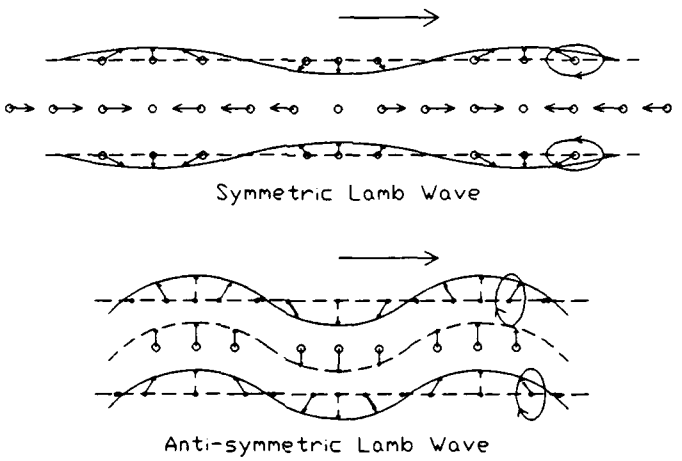

Figure 1.3.4 Representation of particle motion during propagation of symmetric and anti-symmetric Lamb waves.

It should be noted that in Lamb wave propagation particle motion exists throughout the body of the plate, unlike surface Rayleigh waves which are exponentially attenuated in a direction normal to the surface.

As noted earlier, holographic interferometry has proven quite useful in mapping the out-of-plane displacements of an object's surface. Consequently, anti-symmetric Lamb waves, whose primary motion is in the out-of-plane (y axis) direction, are far better suited for holographic interferometry than are the symmetric modes.

1.4 Holographic Theory

Holography possesses the unique ability to record and subsequently reconstruct an optical wavefront[16]. Unlike a photograph, which records only optical

wavefront amplitude information, a hologram records both the optical wavefront amplitude and phase information. In a typical setup for recording a hologram, as shown in Figure 1.4.1, a single beam of coherent light is split into two separate beams. One beam is used to illuminate the object of interest, the second beam directly illuminates a black and white film plate. These beams are termed the object and reference beams respectively.

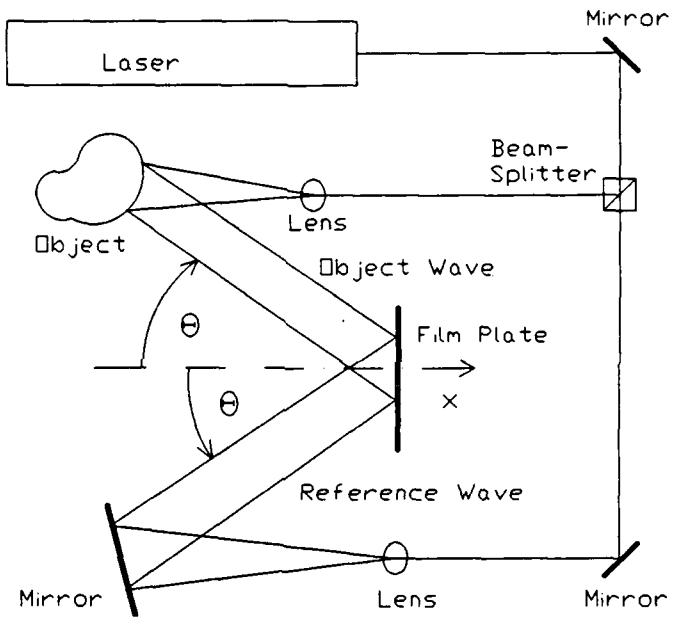

Figure 1.4.1 Schematic of a typical holography setup.

Mathematically, the reference and object wavefronts at the film plane $z=0$ can be described as:

$$\underline{R} = R(x,y)e^{j(kx\sin\theta+\gamma(x,y))} \tag{1.4.1}$$

$$\underline{O} = O(x,y)e^{-j(kx\sin\theta+\phi(x,y))} \tag{1.4.2}$$

where $R(x,y)$ is the amplitude information in the reference wave, θ is the angle that the reference wave makes with the film normal, $\gamma(x,y)$ is the phase information contained in the reference wave, $O(x,y)$ is the amplitude information contained in

the object wave, $(-\theta)$ is the angle that the object wave makes with the film normal, and $\phi(x,y)$ is the phase information contained in the object wave. For a planar reference wave, $\gamma(x,y)$ can be taken as zero, in that there is no phase variation for a plane wavefront.

Since coherent light is used, light which is diffusely reflected from the object interferes with light from the reference wave at the film plate. The interference pattern which results is recorded on the film plate. Since film records wavefront intensity, which is the square of the optical amplitude, it is the square of the sum of the reference and object waves which are recorded:

$$I = |\underline{R} + \underline{O}|^2 = (\underline{R} + \underline{O})(\underline{R}^* + \underline{O}^*) \tag{1.4.3a}$$

$$= R^2(x,y) + O^2(x,y) + R(x,y)O(x,y)e^{j(2kx\sin\theta + \phi(x,y))} \tag{1.4.3b}$$

$$+ R(x,y)O(x,y)e^{-j(2kx\sin\theta + \phi(x,y))}$$

Here, I is the intensity recorded on the film, and (*) denotes the complex conjugate.

Once developed, the film becomes a diffraction grating, consisting of an extremely fine series of black and clear lines, indicating regions where constructive or destructive interference between object and reference waves occurred. The amplitude transmittance *T(x,y)* of the developed hologram is now proportional to this fine diffraction grating. Upon reillumination of the hologram, the incident wavefront is modified according to the transmittance of the hologram. In the case where the reconstructing wave is identical to the original reference wave $\underline{R}$, and defining $\underline{A}$ as the reconstructed wavefront

$$\underline{A} = T(x,y) \cdot \underline{R} \tag{1.4.4}$$

results in the following four terms:

$$\underline{A} = R^3(x,y)e^{j(kx\sin\theta)} \tag{1.4.5a}$$

$$+ R(x,y)O^2(x,y)e^{j(kx\sin\theta)} \tag{1.4.5b}$$

$$+ R^2(x,y)O(x,y)e^{j(3kx\sin\theta + \phi(x,y))} \tag{1.4.5c}$$

$$+R^2(x,y)O(x,y)e^{-j(kx\sin\theta+\phi(x,y))} \qquad (1.4.5d)$$

The first two terms (1.4.5a, 1.4.5b) are transmitted waves which propagate in the $(+x\sin\theta)$ direction and contain only amplitude information (see Figure 1.4.2). The third term (1.4.5c) represents a diffracted wave which propagates in the $(+3x\sin\theta)$ direction, contains both amplitude and phase information, but forms a psuedoscopic image because of the phase reversal. The fourth term (1.4.5d), however, represents a diffracted wave which propagates in the $(-x\sin\theta)$ direction, and contains both the original object wave amplitude ($O(x,y)$) and phase ($\phi(x,y)$) information. It is apparent that this term is identical to the original object wavefront except for a proportionality constant, and it is this term which gives rise to the reconstructed virtual image.

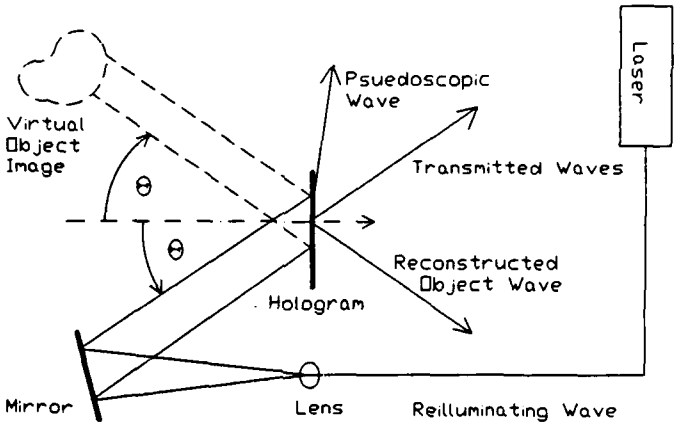

Figure 1.4.2 Schematic of holographic reconstruction.

In many applications, the optical wavefront which is recorded is that from the surface of an object. When such a hologram is reilluminated with the reference beam, the original object wavefront is reconstructed and a virtual image of the object appears at the point in space the object originally occupied. In the case of double exposure holographic interferometry, each film plate records two separate

diffraction patterns. These patterns correspond to two separate exposures of a given test object at different instants in time. When the double exposure hologram is reilluminated, both wavefronts are reconstructed. Since both wavefronts propagate in the same direction and are coherent, they are capable of interfering with each other. Any disturbance to the object surface between the two holographic exposures which causes an optical phase delay between the wavefronts results in an interference pattern superimposed on the object image[17]. The first and second object wavefronts take the form:

$$\underline{O_1} = O(x,y)e^{-j(kx\sin\theta+\phi(x,y))}$$

$$\underline{O_2} = O(x,y)e^{-j(kx\sin\theta+\phi(x,y)+\Delta\phi(x,y))}$$

and upon reillumination of the hologram there are two reconstructed wavefronts, each due to a single holographic exposure:

$$\begin{aligned} & R^2(x,y)\underline{O_1} + R^2(x,y)\underline{O_2} \\ &= R^2(x,y)[O(x,y)e^{-j(kx\sin\theta+\phi(x,y))} + O(x,y)e^{-j(kx\sin\theta+\phi(x,y)+\Delta\phi(x,y))}] \\ &= R^2(x,y)O(x,y)e^{-j(kx\sin\theta+\phi(x,y))}\cdot[1+e^{-j\Delta\phi(x,y)}] \end{aligned} \tag{1.4.6}$$

The result is a wavefront identical to the original object wavefront which is modified by the factor $[1+e^{-j\Delta\phi(x,y)}]$. If the phase relationship between first and second exposures is such that $\Delta\phi(x,y) = (2n+1)\pi$, where n is an integer, then there is destructive interference between the wavefronts which results in a dark fringe. If the phase relationship between exposures is such that $\Delta\phi(x,y) = 2n\pi$ then there is constructive interference between the wavefronts resulting in a bright fringe. In many holographic interferometry applications, the optical phase shift $\Delta\phi(x,y)$ is a result of object motion. In such a case, any object motion between holographic exposures which causes an optical path delay corresponding to a 180° phase shift of the object wave results in complete destructive interference.

For a laser emitting a wavelength of 500nm, the out-of-plane displacement necessary to produce a dark-bright fringe pair approaches 250nm for a coaxial system. If all else remains fixed between holographic exposures, the resulting fringe pattern is an equi-displacement contour map of object surface displacements between exposures.

2 Experimental Design

This study was designed to use full field holographic techniques to gain insight into the spatial propagation of Lamb waves, and characterize such propagation as a function of both plate thickness and material elastic constants. To accomplish this, three different materials were used: 7075 aluminum, 70/30 brass, and 1018 steel. Four samples of brass and three samples of steel and aluminum were obtained. All samples were fifteen centimeters square, and for each material, all samples were of different thickness. The thickness for the test samples is shown in Table 2.1.

Material	Thickness (mm)			
	Plate 1	Plate 2	Plate 3	Plate 4
Aluminum	1.60	2.29	3.36	
Brass	0.21	0.54	1.63	3.21
Steel	1.60	2.31	3.10	

Table 2.1 Sample plate thickness.

One face of each sample was sprayed with a flat white paint in order to provide a uniform diffusely reflecting surface for holography. A 5cm length of black velvet was affixed on the painted surface near an edge of each plate. The velvet served to provide a reference length in the holographic interferogram, so that distances between acoustic wave features could be measured accurately.

A length of 6mm diameter aluminum rod was attached to the center of the unpainted face of each specimen with a cyanoacrylate glue, and this rod-plate assembly was then supported in a fixture which held only the rod, leaving the plate

free. The purpose of the aluminum rod was twofold. First, the rod provided an acoustic delay so that the initial laser pulse could record a hologram of the plate surface at rest, and second, the rod provided a localization of the acoustic excitation of the plate.

In order to produce Lamb waves with amplitudes large enough to cause full fringes to appear in the holographic interferogram, a small amount of chemical explosive (approximately 0.2 mg silver acetelyde) was affixed to the free end of the delay rod. Upon detonation of the explosive, a large amplitude acoustic wave was launched down the length of the rod, causing a step excitation of the plate.

A Quantel pulsed Nd:YAG laser with output in both the visible and infra-red (IR) spectrum was used for explosive detonation and as a coherent light source. The laser was modified such that it was possible to obtain a double pulse output. This was accomplished by taking the Q-switch signal output, passing it through a BNC digital delay pulse generator which returned two temporally separated pulses, and inputing the modified signal to the Q-switch. The BNC delay allowed for a temporal separation between laser pulses ranging from $10\mu s$ to $100\mu s$.

The initial laser pulse served two purposes. First, the infra-red beam was focused onto the explosive attached to the end of the aluminum delay rod, detonating the explosive and launching an acoustic wave down the length of the rod which served to excite the sample. At the same time, the visible beam recorded a hologram of the plate surface at rest.

The second laser pulse recorded a second holographic exposure of the sample surface on the film plate, however in the second exposure the sample surface was distorted owing to the acoustic waves propagating through the plate. A schematic of this system is shown in Figure 2.1.

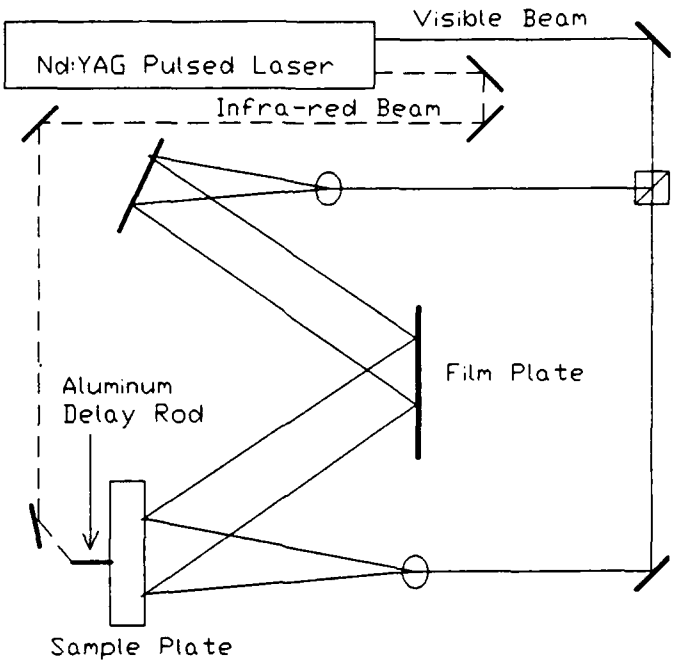

Figure 2.1 Experimental setup for high speed double pulsed holographic interferometry.

For each plate, a series of four or five double exposure holograms was recorded, corresponding to varying time delays between laser pulses. For example, using the medium thickness aluminum plate, the four holograms corresponded to time delays between laser pulses of 45, 52, 59 and 66μs. The acoustic time delay resulting from the aluminum rod was determined to be 35μs, thus the series of double exposure holograms for the medium aluminum plate actually shows the interference pattern caused by the acoustic wave after it has propagated through the plate for 10, 17, 24 and 31μs respectively. The timing between exposures was adjusted separately for each sample in order to obtain the widest possible spread in the propagation distance of the acoustic waves.

Each double exposure hologram was then developed, and the resultant holographic interferograms were reconstructed and digitized using a VICOM digital image processor and stored on disk. Information from the digitized images was then obtained using the VICOM mouse to pinpoint waveform features. Photographs of the holographic interference patterns for the time series mentioned above are shown in Appendix B for aluminum (Figures B.1-B.4). Also shown in Appendix B are representative holographic interferograms for brass (Figure B.5) and steel (Figure B.6).

3 Results and Discussion

As stated previously, the evaluation of elastic properties based on acoustic wave propagation relies upon the accurate determination of acoustic velocity for the characteristic modes which can propagate in the material. For thin plates, the primary modes of acoustic propagation have been shown to be the Lamb modes. Since Lamb wave velocity is a function of frequency and plate thickness, it is necessary to characterize how these factors affect wave propagation, as well as determine the acoustic frequency, plate thickness and acoustic velocity before evaluating the elastic properties of the material.

Holographic records of surface displacements arising from pr(pagating Lamb waves can yield information regarding the velocity of the wave. However, for a spatial signal it is difficult to determine the acoustic frequency; rather, the acoustic wavelength is measured. This is shown in Figure 3.1

It is important to note the method with which the velocity and wavelength were determined for the holographic data. Given a step input to the center of a plate, the response of the plate is initially a large non-propagating central displacement, which gives rise to a propagating wave comprised of the frequency components contained in the initial response. For a dispersive material, the velocity and attenuation of high frequency components is much greater than that of lower frequency components. As a result, the waveform which was recorded in each double exposure hologram is essentially a summation of the large amplitude, low frequency waves which were present in the initial pulse. As such, it was difficult to determine one absolute wavelength and its corresponding phase velocity. Instead, an effective wavelength was calculated for a group of waves, and for this wavelength an effective group velocity was determined.

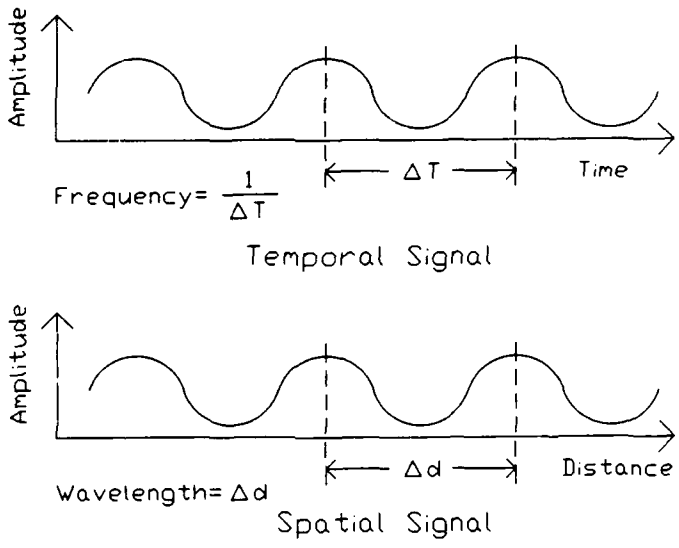

Figure 3.1 Frequency determination for a temporal signal versus wavelength determination for a spatial signal.

For the case of a temporal signal at a single point in space, it has been observed[18] that a technique to determine effective wavelength, frequency, and velocity which yields good correlation between theoretical and experimental results is one in which the effective frequency is calculated based on the inverse time difference between two successive maxima of the temporal signal, and associated with that frequency an effective velocity is determined using the source to detector distance and mean arrival time of the temporally separated peaks. Similarly, it was proposed that for a spatial signal at a single instant in time, an effective wavelength could be determined using the spatial separation of two successive maxima, and that an effective velocity could be determined using the distance from the source of the signal to the spatial mean of the two successive maxima and the time of propagation for the wave. A schematic illustrating this technique is shown in Figure 3.1.

Measurements were made on each holographic interferogram to determine an effective wavelength and a group velocity. Rather than measure an entire wavelength, a half-wavelength, i.e. the distance between the first minima and first maxima, was measured. This was done owing to the fact that in a number of holograms, one complete wavelength could not be determined; the surface displacements had become too small to produce interferometric fringes far from the point of excitation. The velocity was determined by measuring the distance from the point of excitation to the first maxima, and dividing this distance by the time delay between the plate excitation and the second holographic exposure. This is shown in Figure 3.2 Using this technique, results for the aluminum, brass and steel are shown in Tables 3.1, 3.2, and 3.3 respectively.

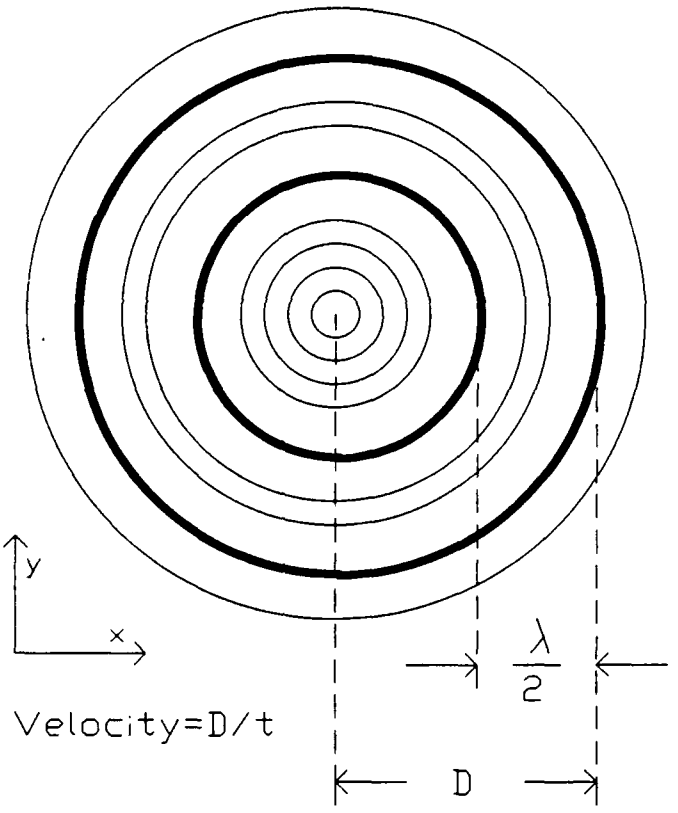

Figure 3.2 Experimental measurement of effective wavelength and group velocity. Wide lines correspond to maxima and minima of the spatial signal. Thin lines represent interferometric fringes resulting from surface displacements.

Thickness (cm)	Delay (μs)	Wavelength (cm)	Velocity (10^5 cm/s)	d/λ
0.160	15	1.125	1.597	0.142
0.160	25	1.915	1.362	0.084
0.160	35	2.511	1.187	0.064
0.160	45	2.969	1.092	0.054
0.229	10	1.197	2.094	0.191
0.229	17	1.535	1.831	0.149
0.229	24	2.116	1.547	0.108
0.229	31	2.614	1.479	0.087
0.229	38	3.021	1.422	0.076
0.336	10	1.481	2.510	0.227
0.336	15	1.597	2.199	0.210
0.336	20	2.199	2.085	0.153
0.336	25	2.573	1.934	0.131

Table 3.1 Results for aluminum plates.

Thickness (cm)	Delay (μs)	Wavelength (cm)	Velocity (10^5 cm/s)	d/λ
0.021	25	0.574	0.467	0.037
0.021	35	0.739	0.385	0.028
0.021	45	0.779	0.342	0.027
0.021	55	0.897	0.291	0.023
0.021	65	0.968	0.269	0.022
0.054	15	0.699	0.841	0.077
0.054	25	0.939	0.715	0.057
0.054	35	1.212	0.623	0.045
0.054	45	1.455	0.556	0.037
0.054	55	1.566	0.509	0.034
0.054	65	1.667	0.466	0.032
0.163	15	0.897	1.256	0.182
0.163	35	1.847	0.914	0.088
0.163	45	2.188	0.818	0.075
0.163	55	2.407	0.745	0.068
0.163	65	2.648	0.681	0.062
0.321	15	1.239	1.529	0.259
0.321	25	2.028	1.438	0.158
0.321	35	2.661	1.271	0.121
0.321	45	3.171	1.165	0.101

Table 3.2 Results for brass plates.

Theoretical Lamb wave dispersion curves were generated for aluminum, brass and steel so that comparisons between the measured velocity/wavelength data and theoretical Lamb wave data could be made. The curves were generated using the FORTRAN program given in Appendix A. Values for the shear and longitudinal wave speeds necessary for the generation of the dispersion curves were experimentally determined using an ultrasonic pulse-echo technique on the thickest sample of each material. The experimentally determined bulk wave velocities are given in

Thickness (cm)	Delay (μs)	Wavelength (cm)	Velocity (10^5 cm/s)	d/λ
0.160	15	1.164	1.595	0.137
0.160	25	1.872	1.174	0.085
0.160	45	2.833	1.016	0.056
0.160	55	3.017	0.905	0.053
0.231	15	1.369	1.812	0.169
0.231	22	2.203	1.714	0.105
0.231	29	2.489	1.499	0.093
0.231	36	2.941	1.371	0.079
0.310	10	1.339	2.301	0.231
0.310	15	1.423	1.994	0.218
0.310	20	2.190	1.942	0.141
0.310	25	2.610	1.799	0.119
0.310	30	2.967	1.728	0.104

Table 3.3 Results for steel plates.

Table 3.4. Figures 3.3, 3.4, and 3.5 plot the theoretical dispersion curves for the lowest order anti-symmetric phase velocities of aluminum, brass and steel, as well as the calculated group velocity curves. The group velocity curves were determined using[19].:

$$v_g = v_p - \lambda \frac{dv_p}{d\lambda} \tag{3.1}$$

Also plotted on the dispersion curve figures are the experimental holographic data given in Tables 3.1, 3.2 and 3.3.

Material	Longitudinal Velocity ($x10^5$ cm/sec)	Shear Velocity ($x10^5$ cm/sec)
Aluminum	6.286	3.070
Brass	4.436	2.110
Steel	5.925	3.188

Table 3.4 Experimentally determined longitudinal and shear wave velocities for material samples.

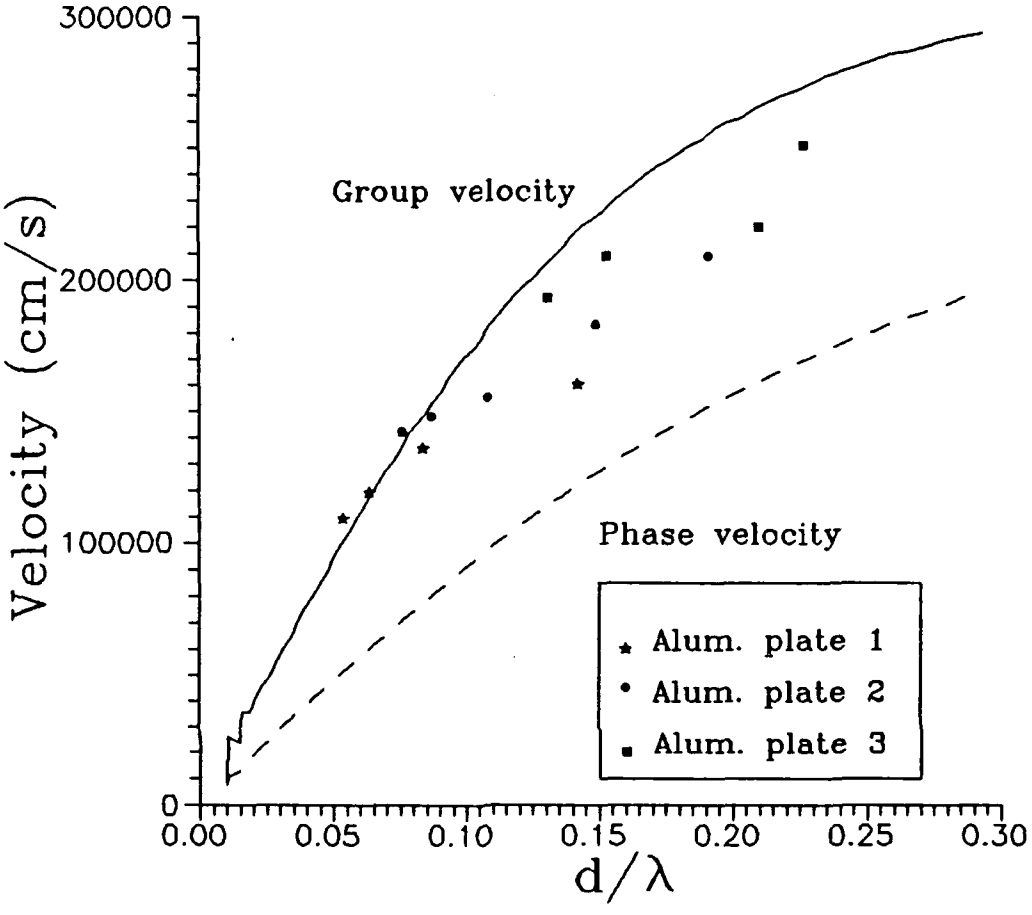

Figure 3.3 Theoretical Lamb wave dispersion curves for phase (dashed line) and group velocity (solid line) of aluminum. Also plotted are the actual experimental data for aluminum.

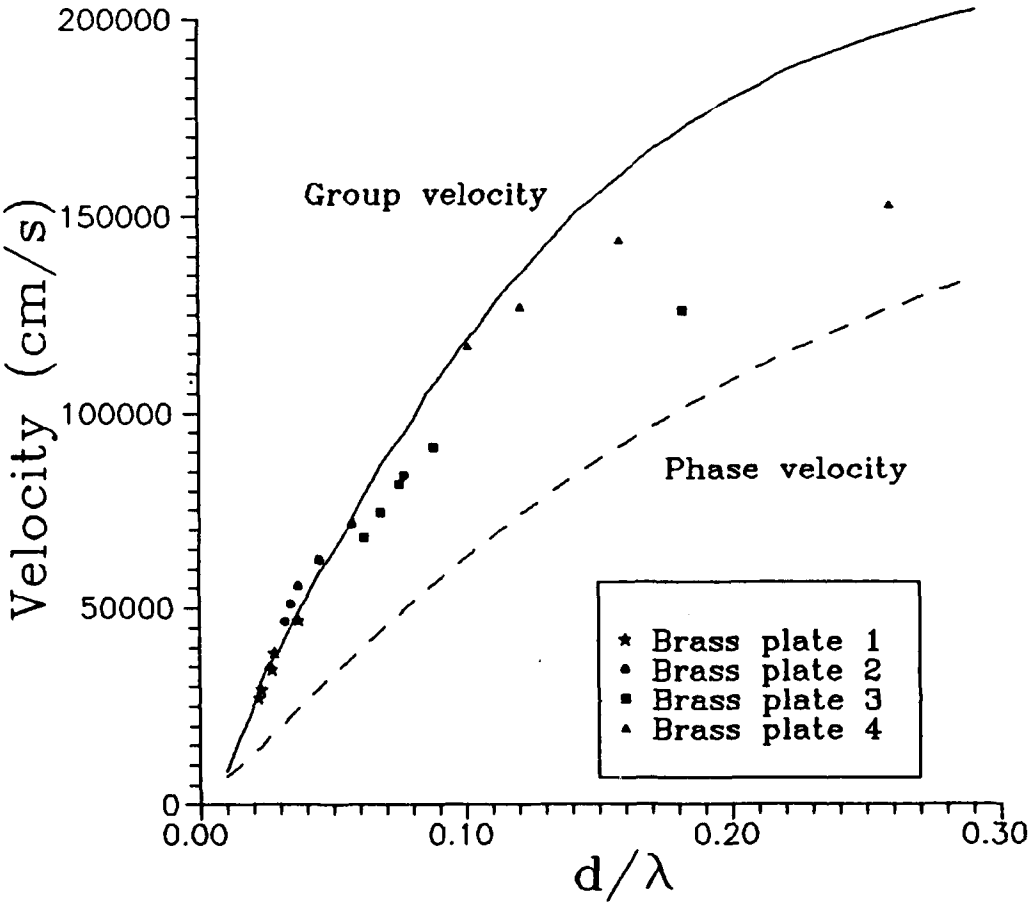

Figure 3.4 Theoretical Lamb wave dispersion curves for phase (dashed line) and group velocity (solid line) of brass. Also plotted are the actual experimental data for brass.

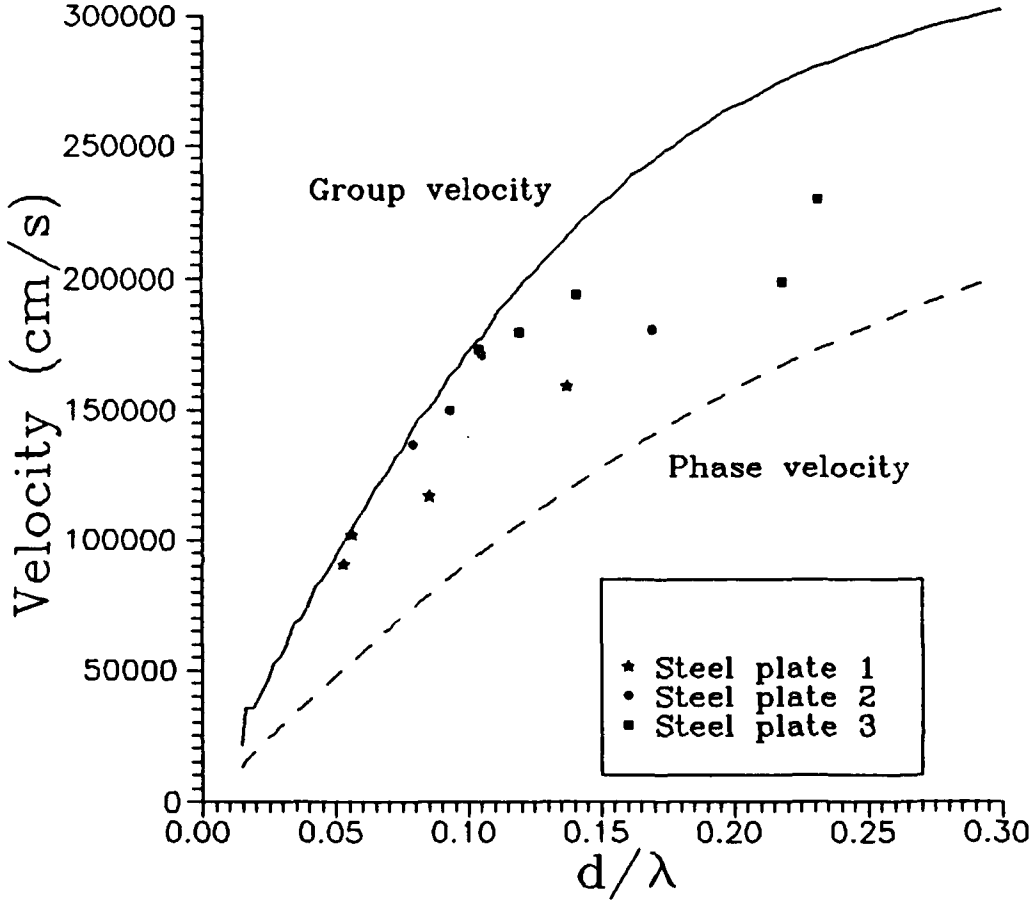

Figure 3.5 Theoretical Lamb wave dispersion curves for phase (dashed line) and group velocity (solid line) of steel. Also plotted are the actual experimental data for steel.

Upon examination of the given dispersion curves for aluminum, brass, and steel, and the associated holographic data, it is evident that for each material, as the ratio d/λ decreases, agreement between theory and experiment increases. In fact, for $d/\lambda < 0.12$, the experimental data and the theoretical group velocity dispersion curves for each material are in excellent agreement. However, as the ratio d/λ increases, experimental estimation of the group velocity deteriorates.

In order to explain the experimental deviation from theory which is apparent at d/λ ratios greater than 0.12, it is necessary to examine the underlying assumptions on which the derivation of Lamb's equation (1.3.11) is based.

The assumption most relevant to this problem, as well as other transient wave phenomena problems, has its basis in the form of the solution chosen for the scalar potential functions ϕ, ψ which must satisfy Equations 1.3.3. In particular, these requirements were met by assuming a solution for the potential functions which were periodic with both time and space. These assumptions yield the Helmholtz conditions as given by Equations 1.3.4, upon which the derivation of the Lamb equation is based.

The assumption of time periodicity in the derivation of the characteristic Lamb equation puts limits on the applicability of the derived dispersion relationship. In effect, the relationship is valid only when the plate motion can be considered periodic or nearly periodic with time. This condition is often termed the steady-state or long time condition, and is satisfied only when the response of the material is no longer affected by the transient non-periodic form of the input. For short times after excitation, when the material response is primarily governed by the local characteristics of the step input, Lamb's theory gives the poorest results. For long times, after the initial effects of the form of the input have damped out, Lamb's theory

yields good results[20]. It has been proposed that on the basis of theory and experiment[21], the critical time interval after which the Lamb wave dispersion relationship is valid is roughly $2(r/v_t)$, where r is the distance from the point of excitation to the point of observation, and v_t is the bulk shear wave velocity.

Similarly, the assumption of spatial periodicity also limits the applicability of the characteristic Lamb equation. As for time periodicity, the derivation of the Lamb dispersion relationship assumes plate motion which is periodic, or nearly periodic, with distance. Local effects of plate loading or excitation are certainly not periodic with distance, and thus the spatial periodicity constraint can be satisfied only far away from the point of excitation, where the material response is essentially unaffected by local loading variations. In actuality, the analysis of a plate's response to step loading needs to be divided into two categories, a near-field solution which must take into account the form of the step and any local non-propagating effects, and a far-field solution where plate motion obeys the spatial periodicity assumption. It has been proposed[22] that the near-field response is confined to a region approximately ten times the plate thickness away from the point of excitation, and that the far-field response is valid further away.

Given the two constraints on the applicability of the characteristic Lamb relationship, namely that the plate response must be periodic with time and space, it is evident that the Lamb dispersion relationship is most effective for determining the far-field, long time response of a plate. Using the far-field, long time criterion, Tables 3.5, 3.6, and 3.7 list the holographic results for aluminum, brass and steel, and note which results fall within the limits of applicability for the dispersion relationship.

Plate thickness (mm)	Time delay (μs)	r/d	$2r/v_t$ (μs)	Far Field	Long Time
1.60	15	10.21	15.6		
1.60	25	14.04	22.2	X	
1.60	35	16.88	27.1	X	X
1.60	45	20.17	32.0	X	X
2.29	10	5.67	13.6		
2.29	17	9.38	20.3		
2.29	24	10.74	24.2	X	
2.29	31	13.46	29.9	X	X
2.29	38	16.16	35.2	X	X
3.36	10	4.67	16.4		
3.36	15	6.85	21.5		
3.36	20	8.54	27.2		
3.36	25	9.96	31.5		

Table 3.5 Experimental results for aluminum detailing which results are valid for far-field, long time response.

Plate thickness (mm)	Time delay (μs)	r/d	$2r/v_t$ (μs)	Far Field	Long Time
0.21	25	32.44	11.1	X	X
0.21	35	37.06	12.8	X	X
0.21	45	45.10	14.6	X	X
0.21	55	45.42	15.2	X	X
0.21	65	50.82	16.6	X	X
0.54	15	13.18	11.9	X	X
0.54	25	20.71	16.9	X	X
0.54	35	25.48	20.7	X	X
0.54	45	29.12	23.7	X	X
0.54	55	33.67	26.6	X	X
0.54	65	36.98	28.7	X	X
1.63	15	7.58	17.8		
1.63	35	12.73	30.3	X	X
1.63	45	14.66	34.9	X	X
1.63	55	16.52	38.8	X	X
1.63	65	17.82	42.0	X	X
3.21	15	4.59	21.7		
3.21	25	7.42	34.1		
3.21	35	9.09	42.2		
3.21	45	10.77	49.7	X	X

Table 3.6 Experimental results for brass detailing which results are valid for far-field, long time response.

Plate thickness (mm)	Time delay (μs)	r/d	$2r/v_t$ (μs)	Far Field	Long Time
1.60	15	10.06	15.1		
1.60	25	11.25	18.4	X	X
1.60	45	18.46	28.7	X	X
1.60	55	20.43	31.2	X	X
2.31	15	7.93	17.1		
2.31	22	10.68	23.7	X	
2.31	29	12.55	27.3	X	X
2.31	36	14.13	31.0	X	X
3.10	10	4.62	14.4		
3.10	15	6.71	18.8		
3.10	20	8.36	24.4		
3.10	25	9.66	28.2		
3.10	30	11.29	32.5	X	

Table 3.7 Experimental results for steel detailing which results are valid for far-field, long time response.

Figures 3.6, 3.7 and 3.8 plot the Lamb wave velocity dispersion curves for phase and group velocities of aluminum, brass, and steel, along with the holographic data which satisfy the far-field, long time criterion.

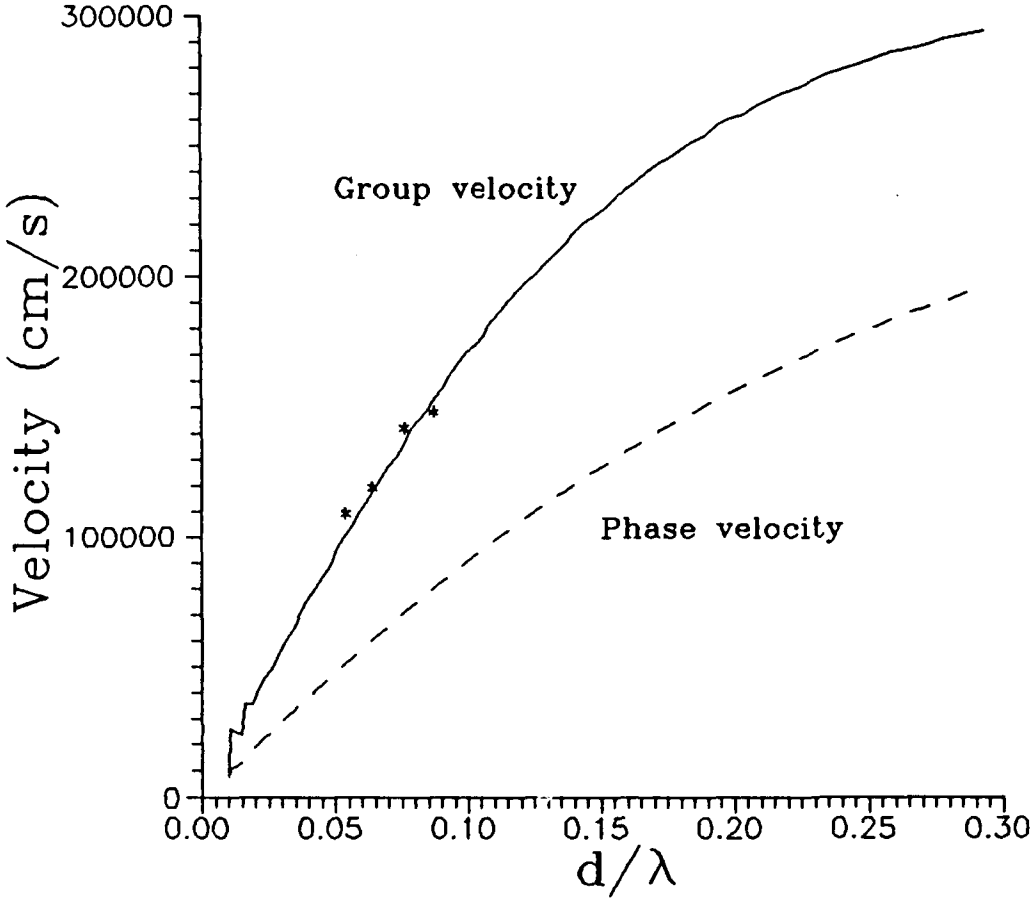

Figure 3.6 Theoretical Lamb wave dispersion curves for phase (dashed line) and group velocity (solid line) of aluminum. Also plotted are the experimental data for aluminum which satisfy the far-field, long time limits of applicability for the Lamb dispersion relationship.

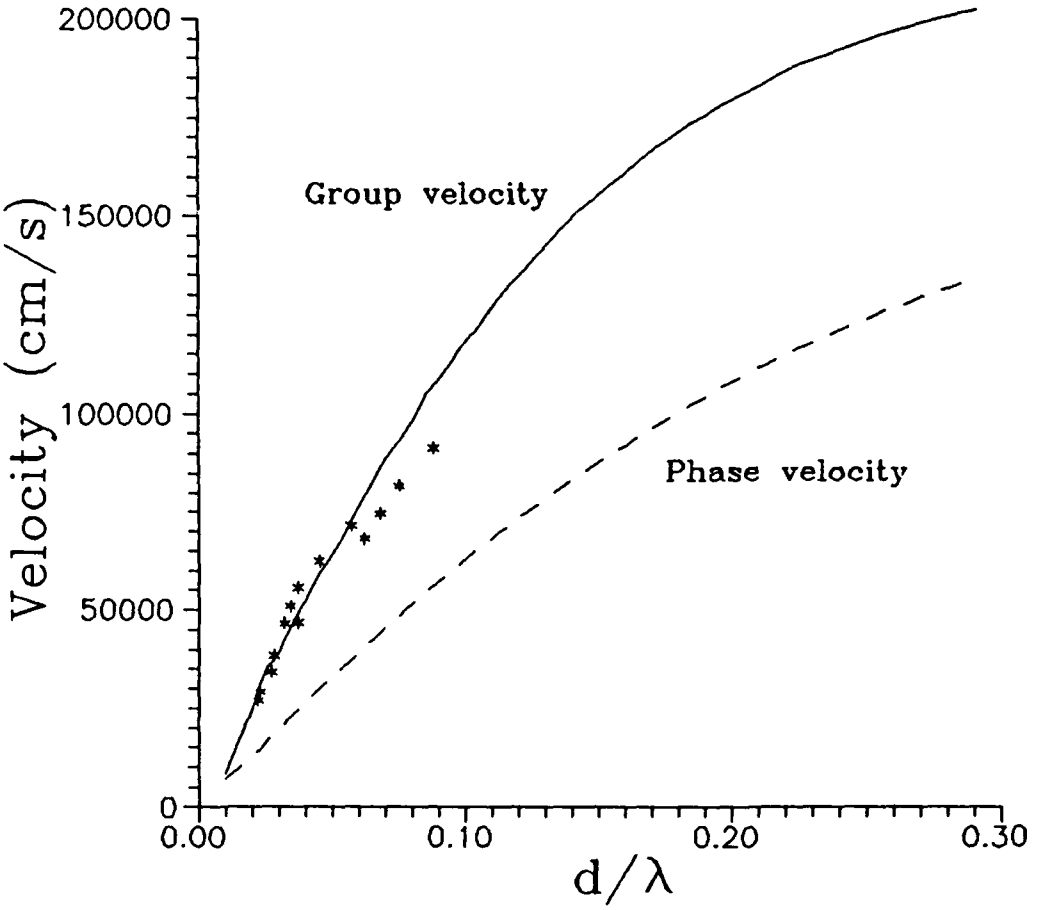

Figure 3.7 Theoretical Lamb wave dispersion curves for phase (dashed line) and group velocity (solid line) of brass. Also plotted are the experimental data for brass which satisfy the far-field, long time limits of applicability for the Lamb dispersion relationship.

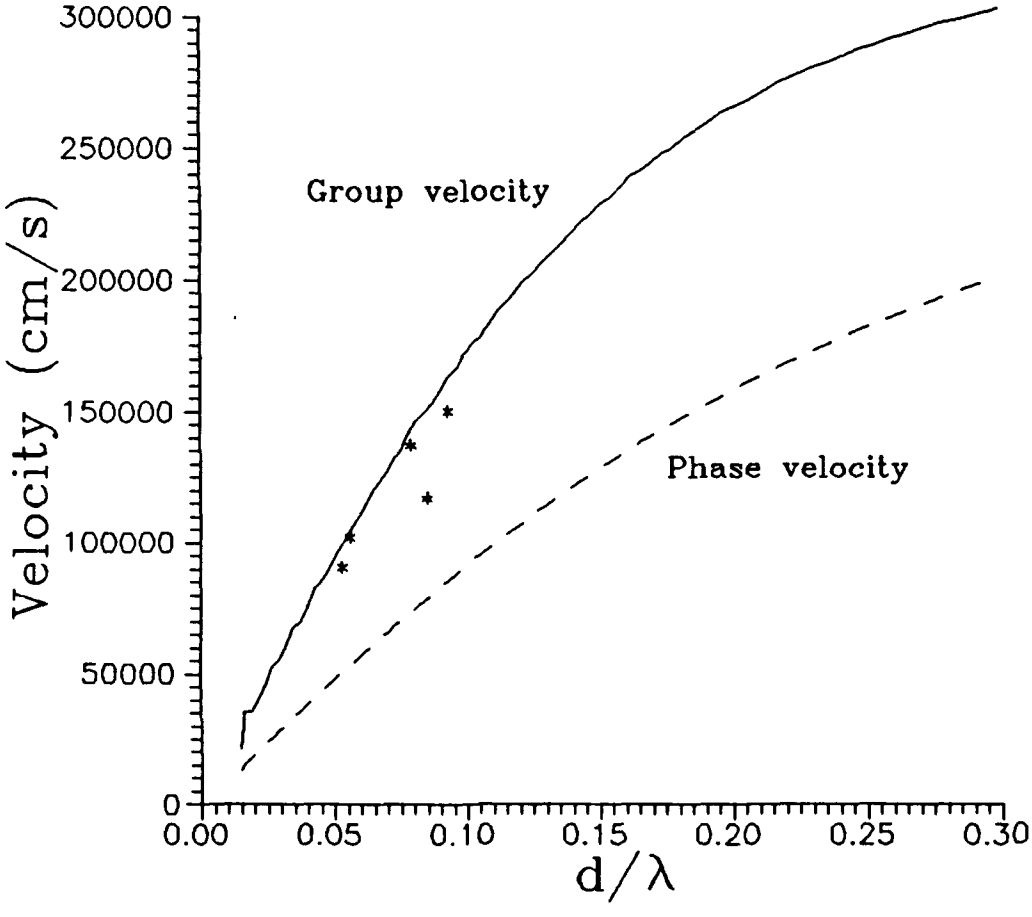

Figure 3.8 Theoretical Lamb wave dispersion curves for phase (dashed line) and group velocity (solid line) of steel. Also plotted are the experimental data for steel which satisfy the far-field, long time limits of applicability for the Lamb dispersion relationship.

Upon examination of Figures 3.6, 3.7 and 3.8 it is clear that the holographic data which falls within the limits of applicability of the Lamb wave dispersion relationship are indeed in good agreement with theory.

Previously it was stated empirically that holographic results for d/λ ratios less that 0.12 were in good agreement with theory. In fact, this is a direct consequence of the long time, far-field limits of applicability for the dispersion relationship. Referring to Tables 3.1, 3.2 and 3.3, it is evident that the experimentally measured Lamb wave wavelengths increase as the time delay between excitation and observation increases. This is a result of the dispersive behavior of the plates. In effect, long times correspond to large measured wavelengths; as time increases, the ratio d/λ decreases.

Taken together, these results show that it is possible to derive a Lamb wave group velocity of a transient propagating plate wave *using holographic techniques* that is in good agreement with elastic theory, provided the results are obtained within the limits of applicability of the characteristic Lamb wave dispersion equation. The technique described uses only features of the spatial waveforms to determine the group velocity, and has been shown to work for different materials and various thickness, given the same measurement criterion for each sample. Owing to the full field nature of holography, it is therefore possible to determine group velocities as a function of d/λ for any direction parallel to the plate surface, and thus to back out material elastic properties for each of these directions.

3.1 Applications

If the elastic properties of a given material are already known, full field holographic techniques offer an excellent means to evaluate the integrity of the sample or detect sub-surface defects. Figure B.5 in Appendix B shows a holographic

interferogram of a propagating Lamb wave in a brass plate. Aside from the fact that the interference pattern is circular, denoting a high degree of isotropy, upon examination of the pattern it is also clear that in the horizontal and vertical directions the Lamb wave amplitude is greater than in the off-axis directions. This can be seen by looking at the first minima of the waveform. Such a variation in amplitude reveals that there is a texture associated with this brass plate: a result of rolling. Consequently, full field mapping of Lamb wave propagation offers a means to qualitatively characterize the stress state of a given material.

Considering that the phase and group velocities of Lamb waves are a function of plate thickness, a local variation in plate thickness should affect the propagation of the wave, and therefore locally alter the holographic interference pattern generated by the plate motion. Because the group velocity decreases with decreasing plate thickness, any thinning of the plate will result in a local retardation of the wave. Figure B.7 in Appendix B shows a holographic interferogram of a transient Lamb wave propagating through a 2.29mm thick aluminum plate. Two holes, one 6mm in diameter and one 13mm in diameter have been milled in the back of the plate to a depth of 1mm. The effect of the holes on the wave propagation are evident. The larger diameter hole affected the wave propagation to a much greater extent than did the smaller hole. This was to be expected, in that the large hole is of comparable size to the acoustic wavelength, whereas the second hole is significantly smaller. Similar techniques could prove extremely useful in composite testing, where a delamination in the interior of a composite plate would reduce the effective plate thickness, and thus retard the wave propagation in the vicinity of the delamination.

In view of the unique ability of Lamb waves to probe the entire thickness of a sample, holographic techniques to map Lamb wave propagation may also prove useful in evaluating the ply orientation of laminar composites, as well as characterizing grossly anisotropic composite structures. Figures C.2, C.3, C.4, C.5 and C.6 show holographic interferograms of propagating Lamb waves in laminar composite plates. Each interferogram corresponds to surface displacements 29 μs after excitation. The series represents five plates, identical in ply lay-up (shown in Figure C.1), but varying in the total number of plies for a given sample. The propagating waves in the composite plates appear to follow the Lamb relationship to some extent; it is clear that as the plate thickness decreases ($n=5 \rightarrow n=1$), so too does the velocity of the wave.

Although the composite plates are certainly not homogeneous or isotropic, and therefore violate the assumptions on which the Lamb wave dispersion relationships were derived, it is possible that in the long wavelength limit the plates may appear homogeneous to the acoustic wave. An indication of the anisotropy associated with the composite plates is, however, exhibited in the Lamb wave velocity. Propagation velocity parallel to the outer plies is clearly greater than the velocity associated with other directions, and is seen to be governed by the orientation of the plies. Indeed, Figures C.6 and C.7 show interference patterns resulting from the propagation of Lamb waves in composite plates of identical thickness, but different ply lay-ups. The composite plate corresponding to Figure C.6 has the ply orientation shown in Figure C.1, whereas the plate corresponding to Figure C.7 has plies of alternating orientation. Comparison of these two figures makes a compelling argument for the possibility of composite materials characterization using holographic mapping of transient acoustic waves.

4 Conclusions

Empirically determined group velocities of transient antisymmetric Lamb modes using holographic mapping techniques have been shown to be in good agreement with predicted results from the elastic theory dispersion relationships for thin plates. The holographic technique uses only features of the propagating waveforms for determination of group velocity, i.e no absolute amplitude information is necessary, and has been applied successfully to materials of different elastic properties and thickness, using the same measurement criterion for each sample.

The existence of limits on the applicability of the characteristic Lamb equation for determination of group velocities given a transient excitation of the plate, as previously proposed, have been experimentally verified. Namely, the time of observation should be greater than twice the distance between the input to the plate and the point of observation divided by the bulk shear wave velocity. Additionally, the minimum observation distance required to be in the far-field of the plate response is approximately ten times the plate thickness.

Finally, the spatial mapping of transient Lamb waves in plates using full field holographic techniques promises to be an excellent tool in the characterization of engineering materials, as well as providing a means of interrogating composite structures for sub-surface defects, delaminations, and gross anisotropy.

APPENDIX A - FORTRAN Program for Generation of Lamb Dispersion Curves

```
c     Program to evaluate lamb wave speed based on
c     ct, cl, kt, d
      real*4 c,ct,cl,c1,c2,c3,c4
      real*4 fd
      integer*4 ibig,istp,ist1,ict,ict1,ict0,ifd
      character*11 fname
c
      write(*,*)' Enter longitudinal bulk wave speed (cm/s): '
      read (*,*) cl
      write(*,*)' Enter transverse bulk wave speed   (cm/s): '
      read (*,*) ct
      write(*,*)' Enter filename to store data : '
      read (*,*) fname
      open(unit=1,file=fname,access='sequential',status='new')
c
      fc1=-1.0
      pi=3.14159
      ifd=1
      istp=10
      ist1=500
      ict1=jint(0.8*ct)
      ict0=jint(0.01*ct)
      ibig=2e9
c
      write(1,*) ' d/l ',' v ',' v/vt '
c
c     run values of c from 0.01ct to 0.8ct in steps
c     of 500 cm/s, then run from 0.8ct to 0.93ct in steps
c     of 0.001ct (30cm/s).
c     At each c evaluate fd
c
 12   do 100, jct=ict0,ict1,ist1
      c=float(jct)
c
      do 50, ict=ifd,ibig,istp
        fd=float(ict)
        c1=tanh(pi*fd*((ct**2-c**2)/(ct**2*c**2))**0.5)
```

```
      c2=tanh(pi*fd*((cl**2-c**2)/(cl**2*c**2))**0.5)
      c3=(2.0-c**2/ct**2)**2
      c4=4.0*((1.0-c**2/cl**2)*(1.0-c**2/ct**2))**0.5
c
      fc=c1/c2-c3/c4
c
      if (fc1*fc) 40,40,50
c
 40   write(1,*) fd/c,c,c/ct
      write(*,*) fd/c,c
      ifd=ict
      goto 100
c
 50   fc1=fc
      continue
 100  fc1=-1
      continue
      if (iflg.eq.1) goto 200
      iflg=1
      ict0=ict1
      ict1=jint(0.933*ct)
      ist1=jint(.0001*ct)
      goto 12
 200  continue
      close(1)
      end
```

APPENDIX B - Holographic Interferograms for Aluminum, Brass and Steel

The following photographs show a time series of holographic interferograms taken for an aluminum plate. Holographic interferograms for brass and steel are similar, and one example of each is shown. The circular interference pattern on each interferogram results from the near isotropy of aluminum, brass, and steel.

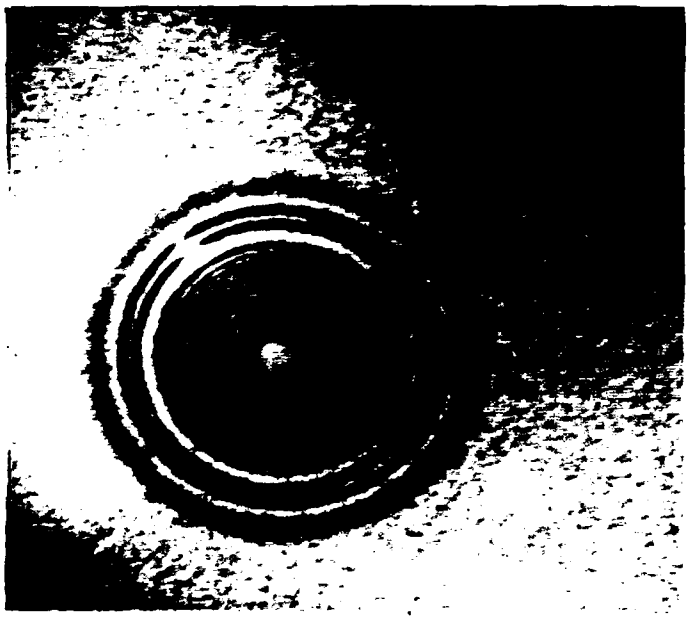

Figure B.1 Holographic interferogram of propagating Lamb wave on a 2.29 mm thick aluminum plate, taken 10 μs after excitation of the plate. The photograph is shown to scale.

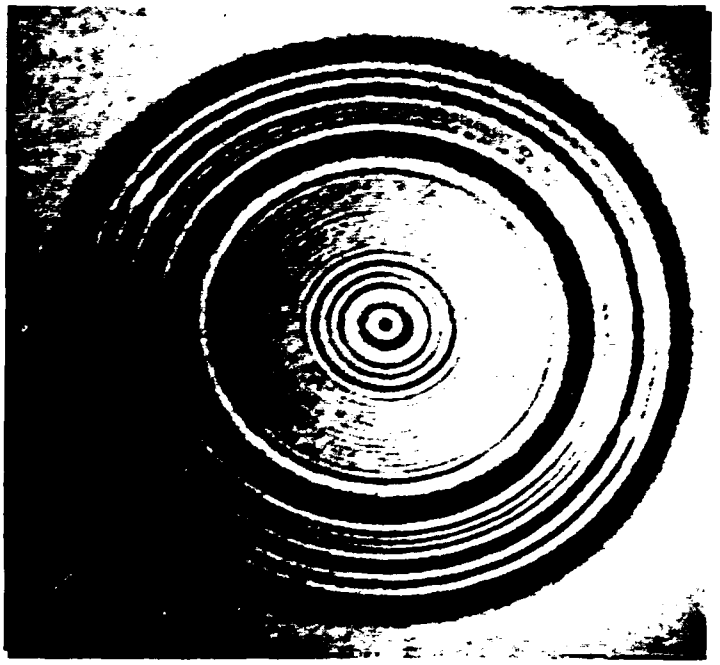

Figure B.2 Holographic interferogram of propagating Lamb wave on a 2.29 mm thick aluminum plate, taken 17 μs after excitation of the plate. The photograph is shown to scale.

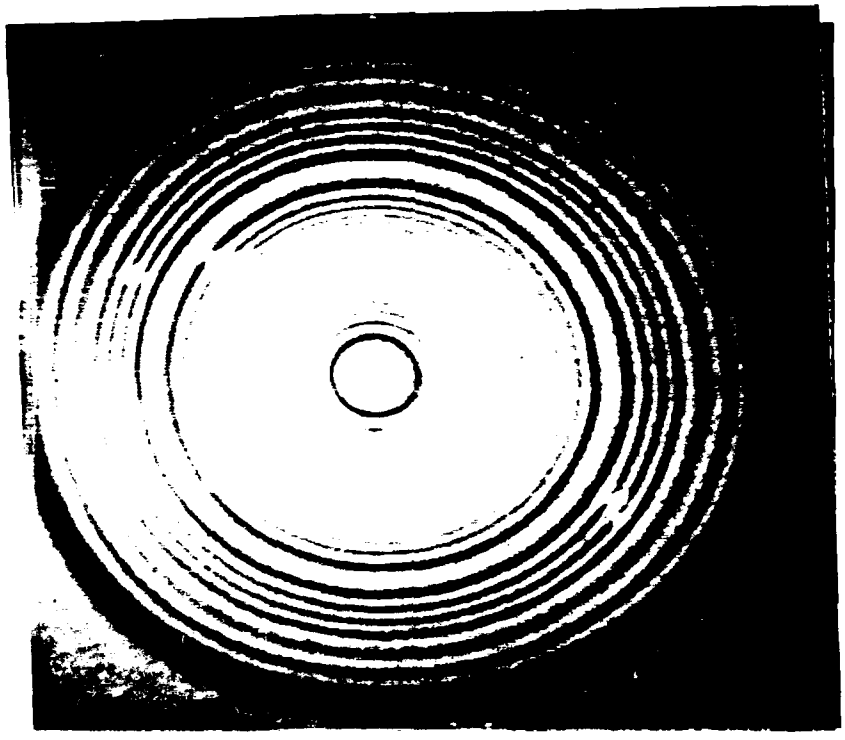

Figure B.3 Holographic interferogram of propagating Lamb wave on a 2.29 mm thick aluminum plate, taken 24 μs after excitation of the plate. The photograph is shown to scale.

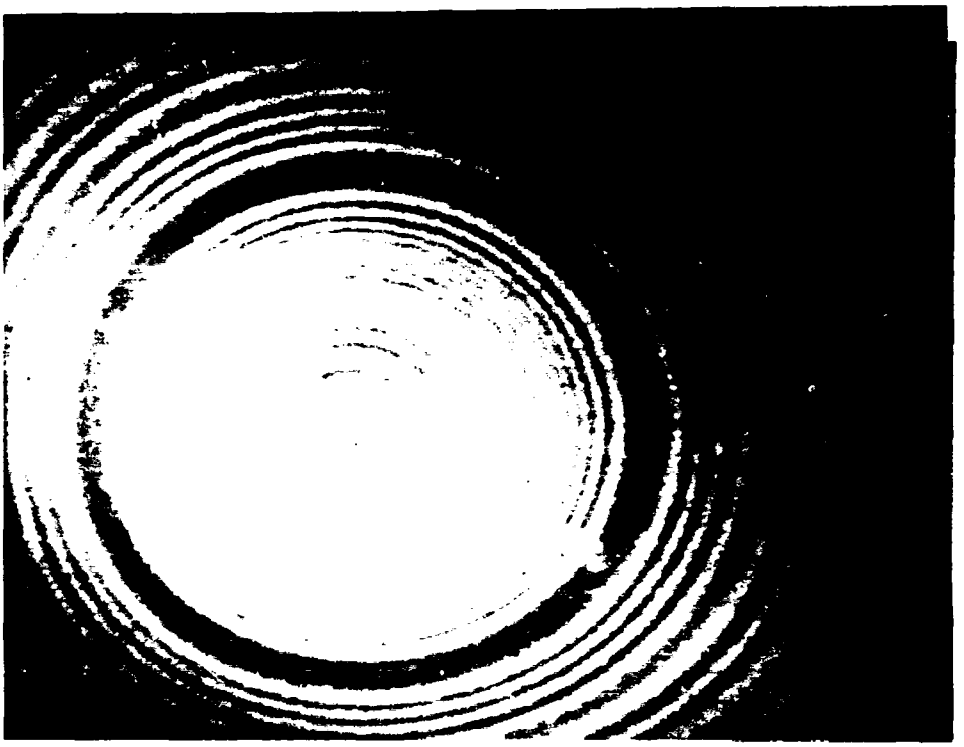

Figure B.4 Holographic interferogram of propagating Lamb wave on a 2.29 mm thick aluminum plate, taken 31 μs after excitation of the plate. The photograph is shown to scale.

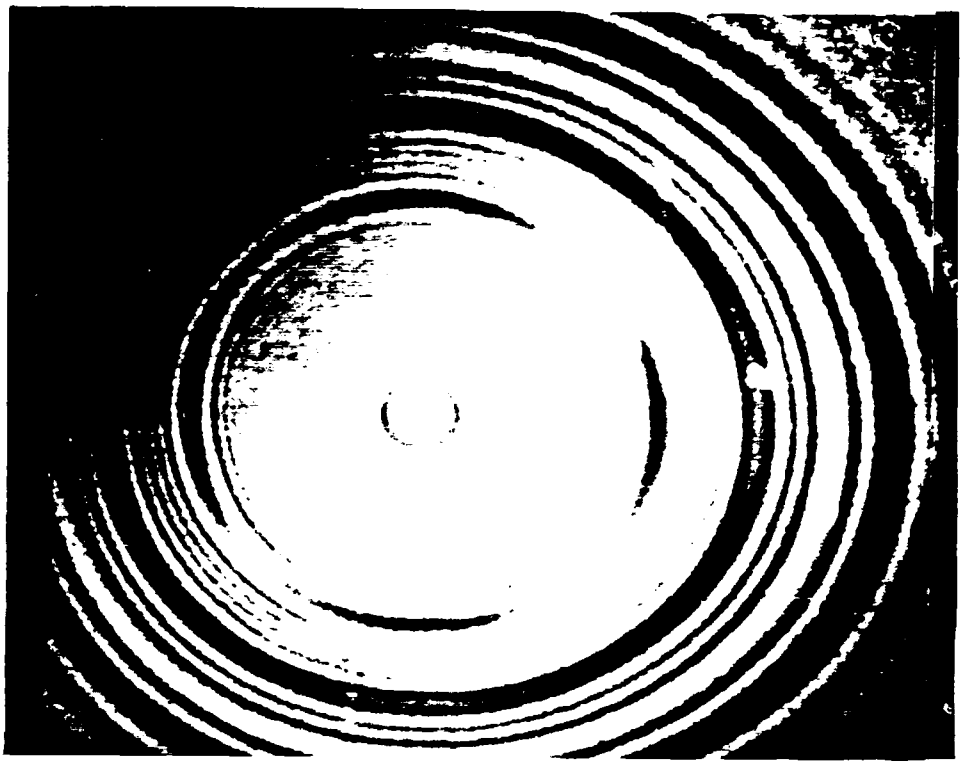

Figure B.5 Holographic interferogram of propagating Lamb wave on a 0.54 mm thick brass plate, taken 45 μs after excitation of the plate. The photograph is shown to scale.

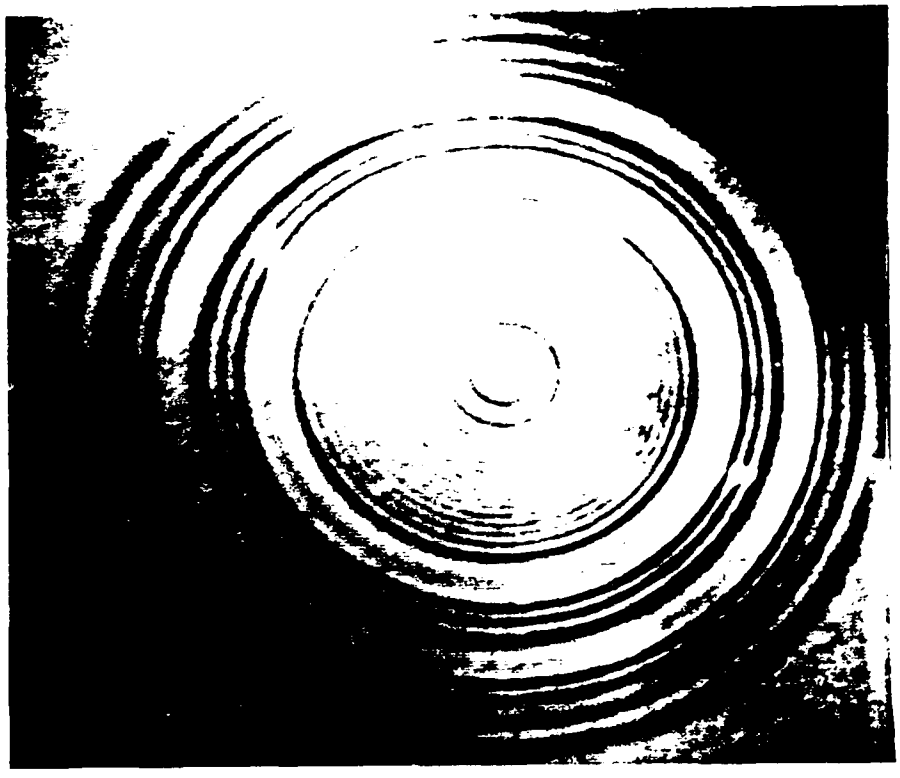

Figure B.6 Holographic interferogram of propagating Lamb wave on a 2.3 mm thick steel plate, taken 22 μs after excitation of the plate. The photograph is shown to scale.

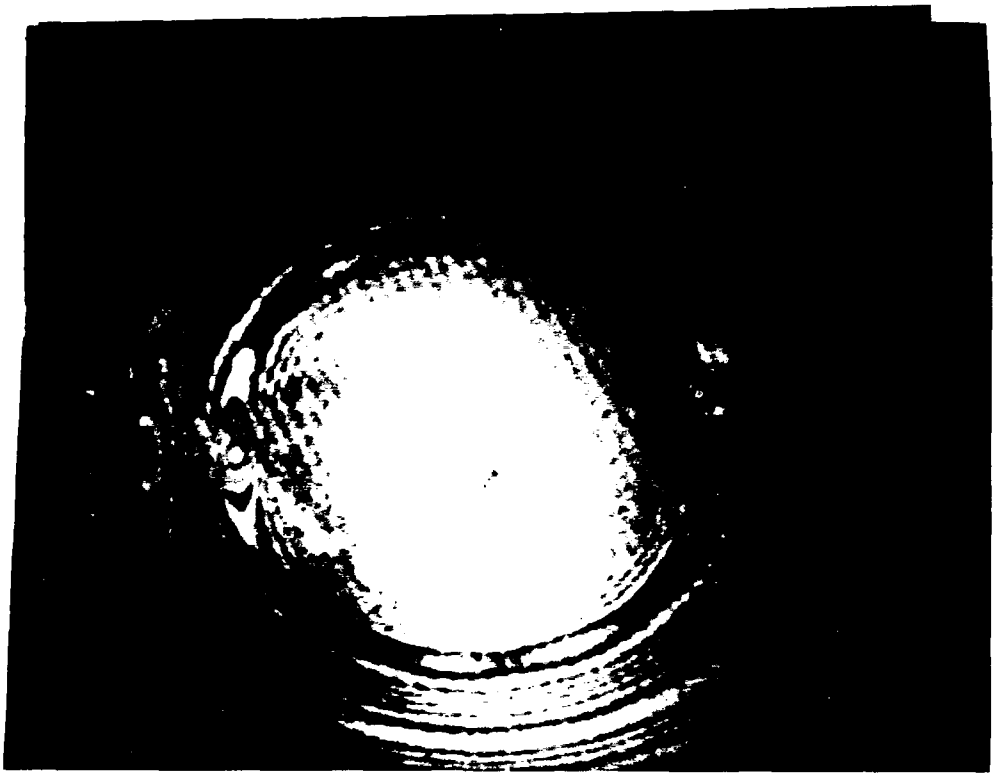

Figure B.7 Holographic interferogram of propagating Lamb wave on a 2.29 mm thick aluminum plate, taken 24 μs after excitation of the plate. The retardation of wave propagation is a result of two holes milled in the back of the plate. The hole on the right half of the plate is 6 mm in diameter, 1 mm deep, and centered 2.5 cm from the center of excitation. The hole in the left half of the plate is 13 mm in diameter, 1 mm deep, and centered 3.2 cm from the center of excitation. The photograph is shown to scale.

APPENDIX C - Holographic Interferograms for Graphite Epoxy Plates

This series of photographs (Figures C.2-C.7) show holographic interference patterns resulting from Lamb wave propagation in laminated composite plates. All plates were manufactured from unidirectional tape prepreg consisting of Toray T-300 graphite fibers impregnated with Fiberite 350°F curing 976 epoxy. The plates corresponding to Figures C.2-C.6 were made with a ply orientation as shown in Figure C.1. All photographs correspond to Lamb wave propagation 29 μs after excitation of the plate.

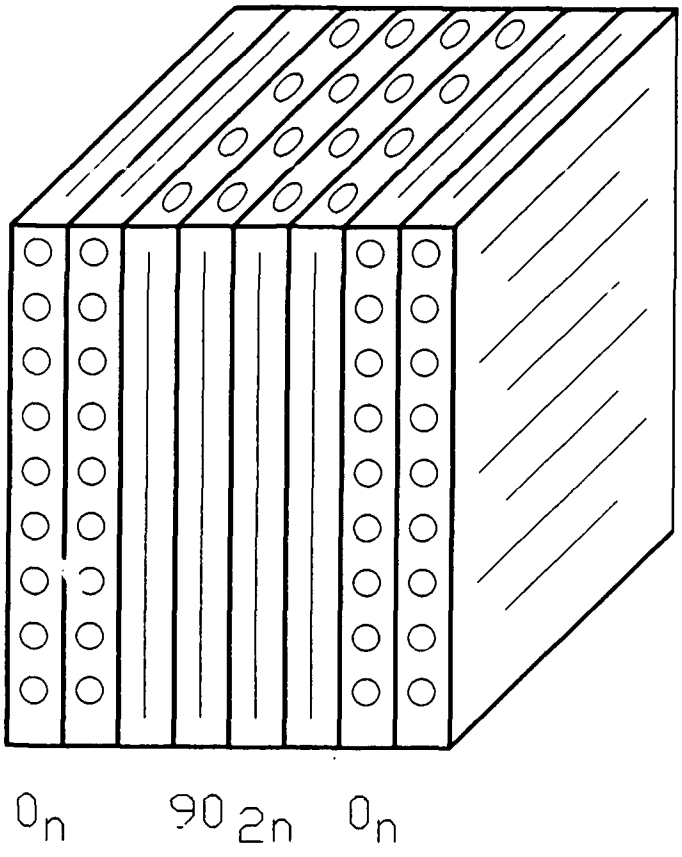

Figure C.1 Schematic illustrating the ply orientation of the graphite epoxy composite plates. The index *n* gives an indication of the number of plies at a given orientation, as shown in the schematic. For the plate shown, n=2, signifying 2 plies at 0° orientation, followed by 4 plies at 90°, ending with 2 plies at 0°.

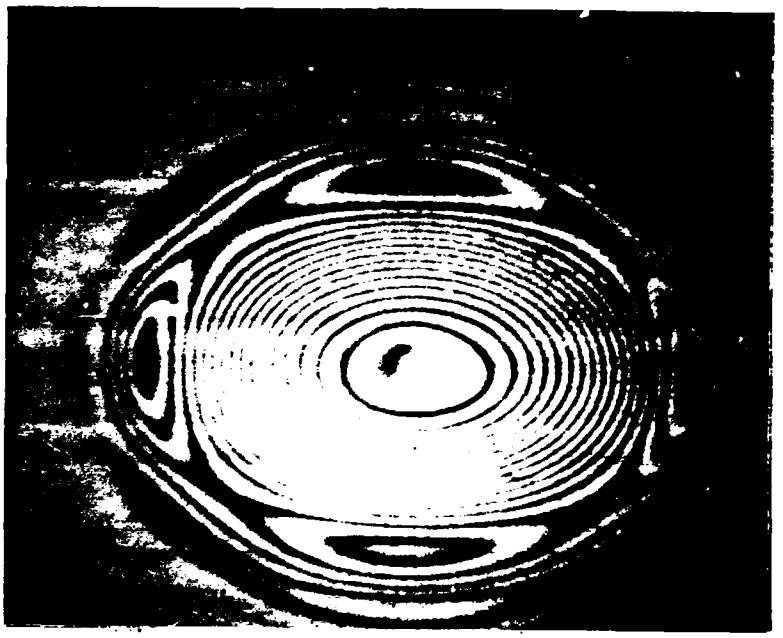

Figure C.2 Holographic interferogram of propagating Lamb wave on a graphite epoxy composite plate with ply orientation index number n=5. The photograph is shown to scale.

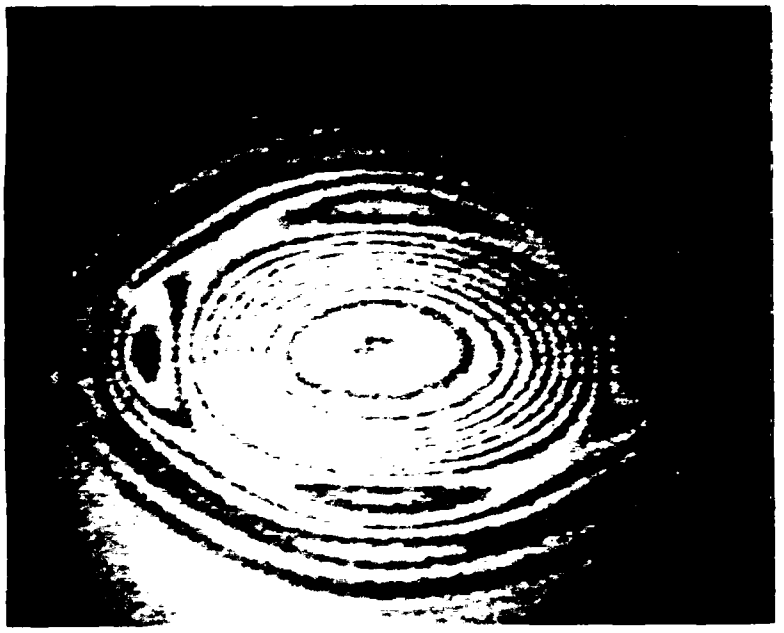

Figure C.3 Holographic interferogram of propagating Lamb wave on a graphite epoxy composite plate with ply orientation index number n=4. The photograph is shown to scale.

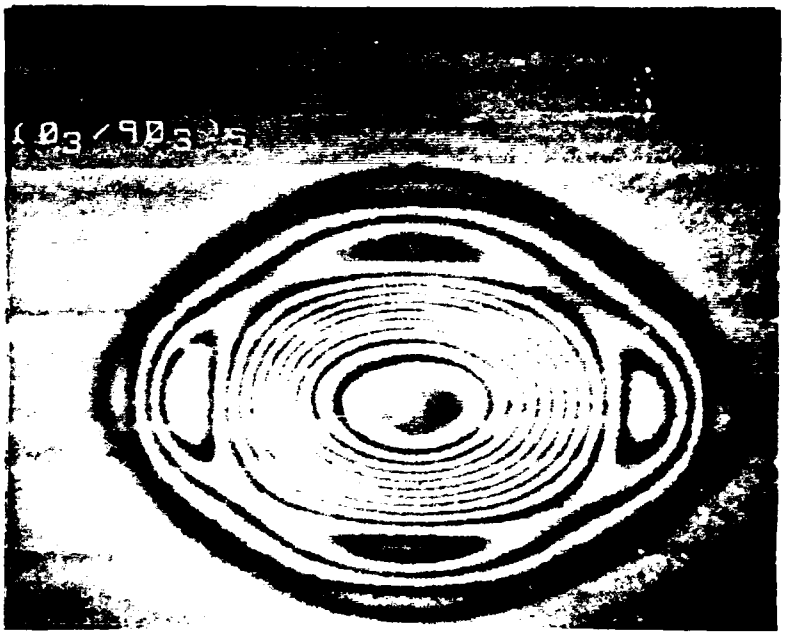

Figure C.4 Holographic interferogram of propagating Lamb wave on a graphite epoxy composite plate with ply orientation index number n=3. The photograph is shown to scale.

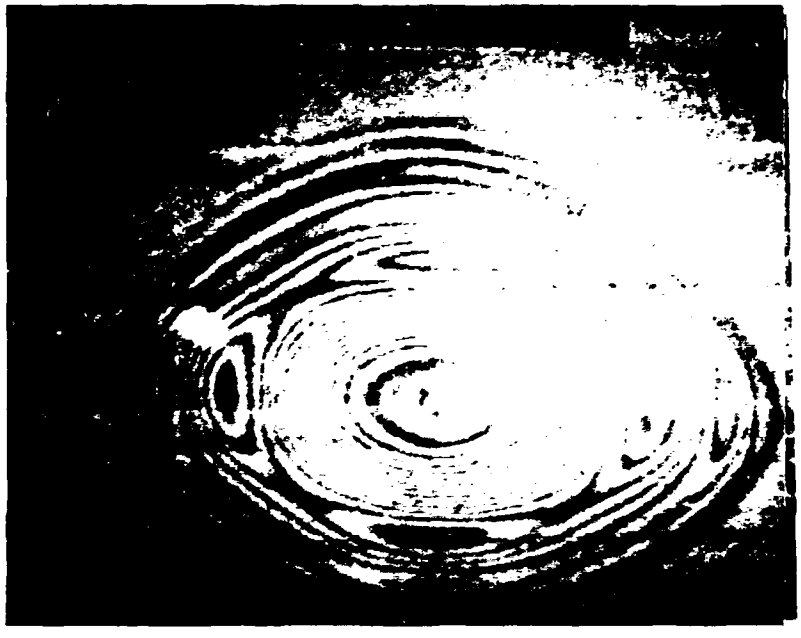

Figure C.5 Holographic interferogram of propagating Lamb wave on a graphite epoxy composite plate with ply orientation index number n=2. The photograph is shown to scale.

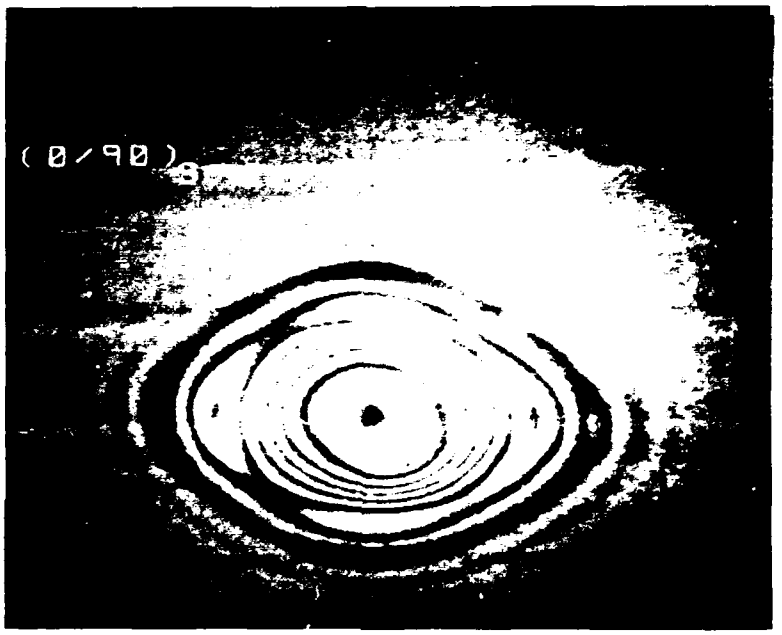

Figure C.6 Holographic interferogram of propagating Lamb wave on a graphite epoxy composite plate with ply orientation index number n=1. The photograph is shown to scale.

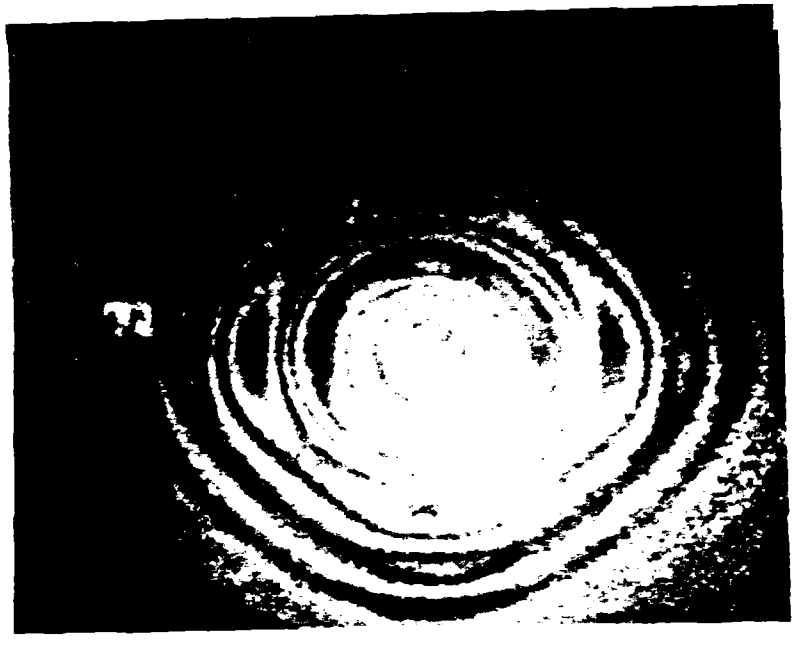

Figure C.7 Holographic interferogram of propagating Lamb wave on a graphite epoxy composite plate with ply orientation given by 0-90-0-90. The photograph is shown to scale.

References

1. R.E. Green, *Treatise on Materials Science and Technology, Volume 3: Ultrasonic Investigation of Materials Properties*, H. Hermann, editor, Academic Press, N.Y. 1973
2. H.J. McSkimin, *Ultrasonic Methods for Measuring the Mechanical Properties of Liquids and Solids*, in *Physical Acoustics, Principles and Methods*, W.P. Mason, editor, vol. 1A, Academic Press, N.Y. 1964
3. M. Redwood, *Mechanical Waveguides*, Pergamon Press, N.Y. 1960, pp.4
4. A.E.H. Love, *A Treatise on The Mathematical Theory of Elasticity*, Cambridge University Press, 1920, pp.97
5. H. Kolsky, *Stress Waves in Solids*, Dover Publications, N.Y. 1963, pp. 13
6. H. Krautkramer & J. Krautkramer, *Ultrasonic Testing of Materials*, Springer-Verlab, N.Y. 1983
7. B.J. Elkind, M. Rosen, H.N.G. Wadley, *Ultrasonic Characterization of Surface Modified Layers*, Metallurgical Transactions, vol. 18A, March 1987, pp.473-480
8. I.A. Viktorov, *Rayleigh and Lamb Waves*, Plenum Press, N.Y. 1967, pp.3
9. Kolsky, pp. 21
10. H. Lamb, *On Waves in an Elastic Plate*, Proceedings of the Royal Society of London, 93A, 1917
11. D.C. Worlton, *Experimental Confirmation of Lamb Waves at Megacycle Frequencies*, Journal of Applied Physics, vol. 32, 1961, pp.967-971
12. D.C. Worlton, pp.967-971
13. Viktorov, pp.70
14. Viktorov, pp.76
15. Krautkramer & Krautkramer, pp.11
16. C.M. Vest, *Holographic Interferometry*, John Wiley & Sons, N.Y. 1979
17. J.P. Waters, in *Holographic Nondestructive Testing*, R.K. Erf editor, Academic Press, N.Y. 1974

18. R.J. Dewhurst, C. Edwards, A.D.W. McKie, S.B. Palmer, *Estimation of the Thickness of Thin Metal Sheet Using Laser Generated Ultrasound*, Applied Physics Letters, vol. 51(14), October 1987

19. Viktorov, pp. 72

20. K.F. Graff, *Wave Motion in Elastic Solids*, Ohio State University Press, 1975, pp. 244

21. M.A. Medick, *On Classical Plate Theory and Wave Propagation*, Journal of Applied Mechanics, vol. 28, 1961 pp. 223-228

22. Y-H Pao, *Transient AE Waves in Elastic Plates*, in "Progress in Acoustic Emission: Proceedings of the 6th International Acoustic Emission Symposium", Japan 1982, pp. 181-197

VITA

[redacted] In May, 1987, he received a Bachelor of Science degree in Biomedical Engineering from the Johns Hopkins University, having also completed all degree requirements for a B.S in Materials Science and Engineering. [redacted]